COUPLED MOORING ANALYSIS OF A CALM BUOY BY A CFD APPROACH

A Thesis

by

HAOYUAN GU

Submitted to the Office of Graduate and Professional Studies of
Texas A&M University
in partial fulfillment of the requirements for the degree of

MASTER OF SCIENCE

Chair of Committee,	Hamn-Ching Chen
Committee Members,	Richard Mercier
	Alan Palazzolo
Head of Department,	Sharath Girimaji

December2016

Major Subject: Ocean Engineering

ABSTRACT

The catenary anchor leg mooring (CALM) system is widely used as an efficient and economic single point mooring system in offshore engineering applications. CALM buoys are often connected to FPSOs with large flowlines for offloading function. Compared to other floating structures like FPSOs or TLP, CALM buoy is more sensitive to the responses of mooring lines and oil offloading lines due to its special characteristics. These features for buoy can result in dangerous motions causing fatigue damage in mooring and flowlines systems. Therefore, it is essential to develop advanced numerical methods for accurate estimate of dynamic motion for CALM buoys.

In this research thesis, the Finite-Analytic Navier-Stokes (FANS) code is coupled with an in-house MOORING3D code for time-domain simulation of the hydrodynamic response of CALM buoy system. In the FANS code, the fluid domain is decomposed into multi-block overset grids. The Large Eddy Simulation (LES) turbulence model is used to provide accurate prediction of vortex-induced motion of the buoy. The mooring system is simulated with a nonlinear finite element module, MOORING3D. An interface module is established to facilitate interactive coupling between the buoy and mooring lines. The coupled FANS/MOORING3D code is calibrated first for free-decay case and compared with model test data. Then the coupled code is applied for the simulation of two degree-of-freedom vortex-induced motion of a CALM buoy in uniform currents to illustrate the capability of the present CFD approach for coupling mooring analysis of offshore structures.

With the study it can be verified that the coupled FANS/MOORING3D method is able to provide an accurate simulation of the hydrodynamic behavior of the CALM buoy system.

DEDICATION

This thesis is dedicated to my beloved parents. Thank you for your consistent support and encouragement all the time.

This thesis is also dedicated to my girlfriend Weiqian. Thank you for your understanding and utmost care from the beginning to the end.

ACKNOWLEDGEMENTS

I would like to offer my sincere gratitude to my committee member chair, Dr. Chen for his patient guidance and persistent support. It's an honor for me to conduct my research under his instruction. I've learned a lot from Dr. Chen in the aspect of both work and life. I would also like to thank my committee members, Dr. Mercier and Dr. Palazzolo for their great support and valuable suggestions for my research.

I would also like to thank the Department of Ocean Engineering for providing the opportunity to improve myself and have a special experience during the past two years. Thank all my friends for their help and encouragement throughout my life at Texas A&M University. Thank Linyue for providing the mooring line analysis code for my research.

I also want to extend my gratitude to the Texas A&M University High Performance Research Computing (HPRC) Center for providing me with the computing resources.

NOMENCLATURE

2D	Two Dimensional
CALM	Catenary Anchor Leg Mooring
CFD	Computational Fluid Dynamics
charl	Characteristic Length
charu	Characteristic Velocity
C_S	Smagorinsky's Coefficient
D	Outer Diameter of Buoy
E	Young's Modulus
FANS	Finite Analytic Navier-Stokes
FEM	Finite Element Method
Fn	Froude Number
FPSOs	Floating Production Storage and Offloading vessels
KG	Center of Gravity above Keel
LES	Large eddy simulation
OOLs	Oil Offloading Lines
RANS	Reynolds-Averaged Navier-Stokes
Rxx	Rotational Mass Moment of Inertia about X-axis
Ryy	Rotational Mass Moment of Inertia about Y-axis
TLPs	Tension Leg Platform
VIM	Vortex-induced Motion

TABLE OF CONTENTS

Page

LIST OF FIGURES

Page

LIST OF TABLES

Page

CHAPTER I

INTRODUCTION AND LITERATURE REVIEW

As an efficient and economic single point mooring system, the catenary anchor leg mooring (CALM) system is now widely used in many areas (Sagrilo et al., 2002). CALM buoys, which are often connected to FPSOs with two or three large flowlines, are very popular nowadays in the deep water areas like West Africa oil fields for the offloading purpose (Duggal et al., 2005). More than 300 systems are being used since the first one was deployed in the 1960's (Williams et al., 2013). Compared to other floating structures like FPSOs or TLP, CALM buoy is more sensitive to the response of mooring lines and oil offloading lines (OOLs) due to its considerably smaller inertia, damping and hydrostatic stiffness. These features of buoy can result in dangerous motions which may cause fatigue damage in mooring and flowlines systems. That's why the accurate estimation of dynamic motion for CALM buoys is very essential (Ryu et al., 2005).

Different methods have been applied to predict the dynamic response of CALM buoy. In model experiments, the whole system is often tested together. Depending on many factors like basin facilities and experimental objectives, the models are designed with different scale ratios and components. In the experiment at MARINTEK's Model Basin, a complete system was considered for simulation, including mooring lines, hawser, buoy and tanker (MARINTEK, 1989). In MARIN's offshore basin, a buoy only with truncated mooring system was studied, in order to test the buoy's characteristics

and effect of waves on the system (Bunnik et al., 2002).For the CALM buoy JIP experiment conducted by Principia R.D., as its focus was on the hydrodynamic behavior of the buoy, only a scaled buoy model was used to take the captive and forced oscillation tests (Ricbourg et al., 2006).

Along with scaled model tests, numerical methods are also used for dynamic analysis. In contrast with the model test, numerical method often studies the buoy and mooring system separately. Most of the numerical methods resort to empirical correlations to solve specific problems. In case of buoys, empirical correlations for lift, drag and added mass based on radiation/diffraction theory and Morrison's equations are often used for the estimation of load on them (Ryu et al., 2005; Sagrilo et al., 2002). The results got from numerical methods are usually compared with the model test results for validation. Forced oscillation tests are frequently used to validate specific hydrodynamic characteristics of the buoy model, such as the added mass and the damping coefficients (Cozijn et al., 2005; Huang et al., 2005; Ricbourg et al., 2006). Free-decay tests and under wave condition tests are commonly conducted to validate the prediction of combined buoy and offload oil lines system. The results of under wave condition tests are mostly expressed in the form of frequency domain (Cunff et al., 2007; Hiraishi et al., 2008; Salem et al., 2012).

To analyze the mooring lines numerically, it's common to regard the cable as a slender rod without bending stiffness and use finite element method to resolve the rod. Different methods are applied to simplify the mooring lines into different numerical mooring models ,like lumped mass method (Bunnik et al., 2002) and nonlinear springs

replacement method (Sagrilo et al., 2002).To validate the numerical model, model tests for mooring lines are conducted as well. Due to the limitation of water depth in wave basins, different methods are used to determine the length of the truncated cables which are used to model the mooring systems in prototype scale(Chen et al., 2000; Hiraishi et al., 2008; Kitney et al., 2001).A fully dynamic coupled or a quasi-static coupled simulation is often used to combine the buoy part together with the mooring system part together (Cozijn et al., 2004).

A few papers also mention CFD method as a way to compute the dynamic behaviors of deep water buoy, while few papers use this method as a main approach for simulation. As CFD is good at simulating the fluid properties, it is used to predict some specific hydrodynamic characteristics of the buoy and compare the result with other methods, like a forced heave motion model test to evaluate the scaling effect on a buoy model (Berhault et al., 2004). Since mooring lines cannot be analyzed by CFD method, some other aiding tools like AQWA-NAUT are used as supplementary to simulate the mooring system part (Woodburn et al., 2005).

The aim of the study in the thesis is to simulate the dynamic behaviors of a CALM buoy system with the help of a combination of CFD code and MOORING3D code. A model test which had been conducted before (Ryu et al., 2006) is simulated numerically. Two sets of experiments were conducted, including a free-decay test and a test under uniform current condition. The first test is to calibrate the numerical model established in the coupled code. The second test is to validate the accuracy of prediction under the current condition by comparing the results with Orcaflex.

The present simulation of CALM buoy system is divided into two parts. The buoy part is modeled and simulated with FANS code. The mooring lines part is modeled and simulated with MOORING3D code. The results from two parts is combined together with an interface module transferring essential information to each other.

CHAPTER II

NUMERICAL APPROACH

The present numerical simulation of CALM buoy system is divided into two parts. The buoy part is modeled and simulated with the FANS code. The mooring lines part is modeled and simulated with MOORING3D code. The results from two parts are combined together with an interface module transferring essential information to each other.

This chapter introduces the numerical approach used for the simulation of CALM Buoy. The theory of MOORING3D, FANS method and interface module between buoy and mooring lines are also mentioned in different sections of this chapter.

MOORING3D

Background

MOORING3D is a cable dynamic analysis code developed by Zhao(Zhao, 2014). It is based on a nonlinear Finite Element Method (FEM) theory. The theory was originally introduced by Garrett(Garrett, 1982) to solve inextensible line problems. And it was then developed further to analyze rods with small elongations and sea bottom effects(Ma et al., 1994), which is the original version of CABLE3D code. On the basis of previous research, Chen modified the original CABLE3D code by including large elongation elements and no bending stiffness (Chen, 2002),and verified that the modified mooring principle is more efficient and trustworthy. MOORING3D is a Fortran 90 code

developed mainly by Zhao based on the theory similar to the improved CABLE3D code(Chen, 2002) and it was modified for the purpose of this research in order to couple with FANS.

In this study, the mooring chain is treated as a long slender structure neglecting bending moments and shear forces. The mainly force is tension along the direction of cable.

Based on the motion equation of a cable in Cartesian coordinate (Lindahl et al., 1983), the governing equation describing the motion of a cable can be deduced as

$$\left(\tilde{\lambda}\mathbf{r}'\right)' + \mathbf{q} = \rho\ddot{\mathbf{r}} \tag{1}$$

where

$$\tilde{\lambda} = \frac{T}{1+\varepsilon} \tag{2}$$

$$\varepsilon = \frac{T}{EA} \tag{3}$$

where T is the tension tangential to cable's direction. $EA$is the elastic stiffness of the cable. **r** is a vector to describe the configuration of the cable, which is a function of the deformed arc length of cable s and time t, and is shown in Figure 1. **q** stands for external force per unit length. $\rho$is the mass of the cable per unit unstretched length.

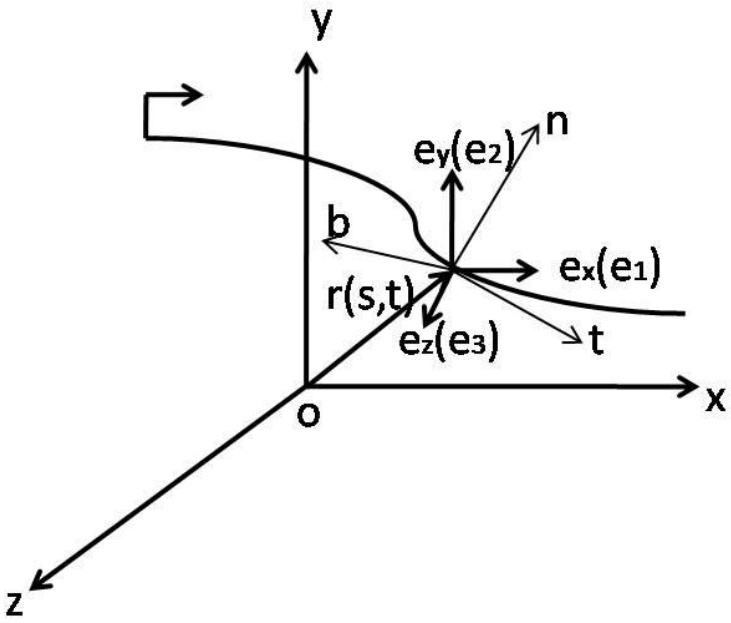

Figure 1. Coordinate System

The external forces **q** is composed of hydrostatic, hydrodynamic and gravity forces. The gravity force is expressed like

$$\mathbf{q}_t(s,t) = -\rho_t g A_t \mathbf{e}_y \tag{4}$$

The hydrodynamic force is divided into added-mass force, drag force and Froude-Krylov force. The added-mass force and drag force can be predicted with Morrison equation.

After dividing the external force into these three parts, the governing equation becomes

$$\mathbf{M}\ddot{\mathbf{r}} - \left(\tilde{\lambda}\mathbf{r}'\right)' = \mathbf{q} \tag{5}$$

where

$$\mathbf{M} = \rho_f A_f \mathbf{I} + \rho_f A_f C_{Mn}(1+\varepsilon)\mathbf{N} + \rho_f A_f C_{Mt}(1+\varepsilon)\mathbf{T} \tag{6}$$

$$\begin{aligned}\mathbf{q} = {} & \left(\rho_f A_f - \rho_t A_t\right) g \boldsymbol{e}_y + \rho_f A_f (1+\varepsilon)(\mathbf{I} + C_{Mn}\mathbf{N} + C_{Mt}\mathbf{T})\mathbf{a}_f \\ & + \frac{1}{2}\rho_f D_f C_{Dn}(1+\varepsilon)\mathbf{N}(\mathbf{v}_f - \dot{\mathbf{r}})\left|\mathbf{N}(\mathbf{v}_f - \dot{\mathbf{r}})\right| \\ & + \frac{1}{2}\rho_f D_f C_{Dt}(1+\varepsilon)\mathbf{T}(\mathbf{v}_f - \dot{\mathbf{r}})\left|\mathbf{T}(\mathbf{v}_f - \dot{\mathbf{r}})\right|\end{aligned} \tag{7}$$

$$\mathbf{T} = \frac{\mathbf{r}'^{r}\mathbf{r}'}{(1+\varepsilon)^2} \tag{8}$$

Besides, the configuration vector **r**must obey the stretching constrain equation:

$$\mathbf{r}' \cdot \mathbf{r}' = (1+\varepsilon)^2 \tag{9}$$

which can also be interpreted as

$$\mathbf{r}' \cdot \mathbf{r}'(1-\tilde{\varepsilon})^2 = 1 \tag{10}$$

with

$$\tilde{\varepsilon} = \frac{\tilde{\lambda}}{EA} \tag{11}$$

With governing equation (Eq. 5) together with rod constraint equation (Eq. 10), the foundation of predicting the hydrodynamic behavior of cable with large elongation and no bending stiffness is established. By applying Galerkin's method to discretize the partial differential terms and Hermite cubics/quadratics shape functions to discretize the coefficients in summation form, these two equations become

$$\gamma_{ikm} M_{njm} \ddot{u}_{kj} + \beta_{ikm} \tilde{\lambda}_m u_{kn} = \mu_{im} q_{mn} + f_{in} \tag{12}$$

and cable constraint equation

$$\frac{1}{2}\beta_{ikm} u_{in} u_{kn} + \frac{1}{2}\tilde{\eta}_{iklm}\left(-2\tilde{\varepsilon}_l + \tilde{\varepsilon}_l{}^2\right)u_{in} u_{kn} - \frac{1}{2}\tau_m = 0 \tag{13}$$

As the unknowns of original Eq.5 and Eq. 10 are $\mathbf{r}$ and $\tilde{\lambda}$, for the two modifiedequations,Eq.12 and Eq. 13, unknowns are$\ddot{u}_{kj}$,u_{kn} and $\tilde{\lambda}_m$, where j, m and n are from 1 to 3 and i, k are from 1 to 4. After applying the boundary conditions, the modified equations can be written in a matrix form as $\mathbf{A}\delta\mathbf{x} = \mathbf{b}$,with$15 + 8(N - 1)$ independent equations to describe the line with N elements in three dimensions. For more detailed information about the derivation, please refer to (Chen, 2002).

This method has been proved efficient in predicting the hydrodynamic response of the cables. To verify whether the MOORING3D code works or not, a prescribed motion test is conducted. The test's results are compared with the results from commercial software Orcaflex under the same experimental condition.

Verification

The verification test consists of a 4-leg 90°spaced mooring lines. The plan and side views of the experimental configuration are shown in Figure 2 and Figure 3. The parameters of the four mooring lines are shown in Table 1. The coordinates of lines' top-end points from Line 1 to Line 4 in x-y plane are (8.5,0), (0,8.5), (0,-8.5), (-8.5,0). The coordinates of lines' bottom-end points from Lines1 to Line 4 in x-y plane are (330,0), (0,330), (0,-330), (-330,0).

Table 1. Parameters of Mooring Line in Verification Test

	Unit	Mooring
Water Depth	m	106.8
Length	m	350
Diameter	m	0.12
EA	N	3.538991012E10
Density	kg/m^3	8841.9413
Normal C_D		1
Normal C_M		2
Axial C_D		0
Axial C_M		1

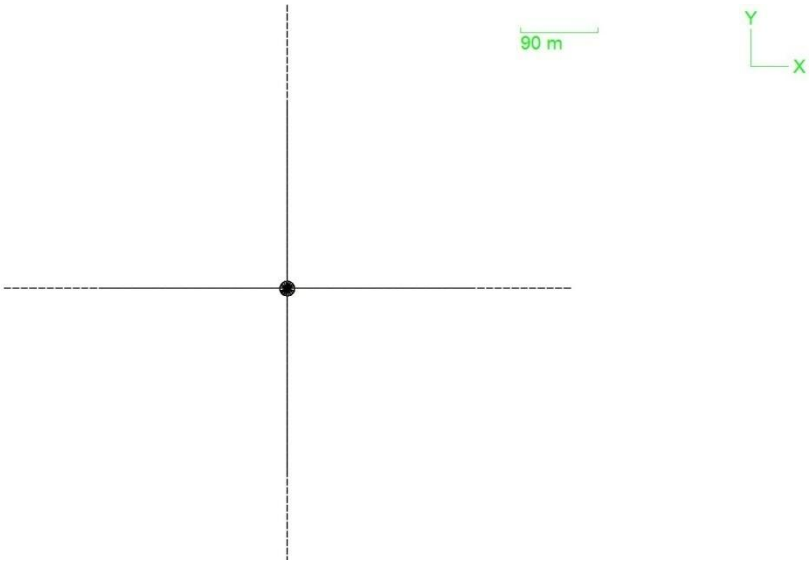

Figure 2. Plan View of Mooring Lines Configuration

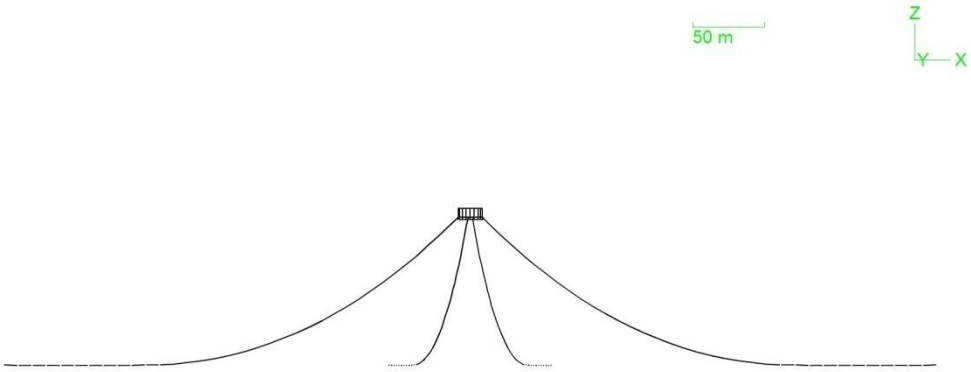

Figure 3. Side View of Mooring Lines Configuration

The test is first simulated in the commercial software Orcaflex. A free-decay test is used to generate the motion of the buoy together with the fairlead of four mooring lines. The initial displacement of the buoy is -8m. The motion curve of the buoy's center of gravity is shown in Figure 4 and Figure 5 in x and y directions. The motion data of four fairleads is used as the displacement input for the MOORING3D code to simulate a prescribed-motion test for the mooring lines.

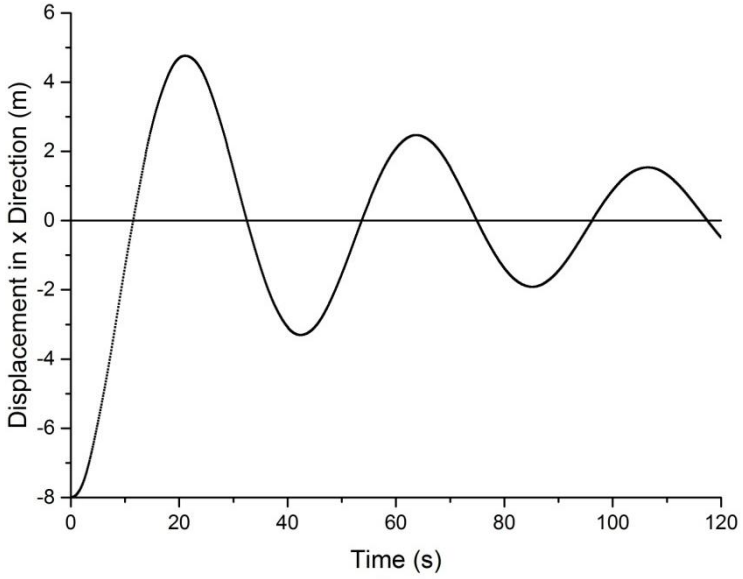

Figure 4. Displacement of Buoy's Center of Gravity in x Direction

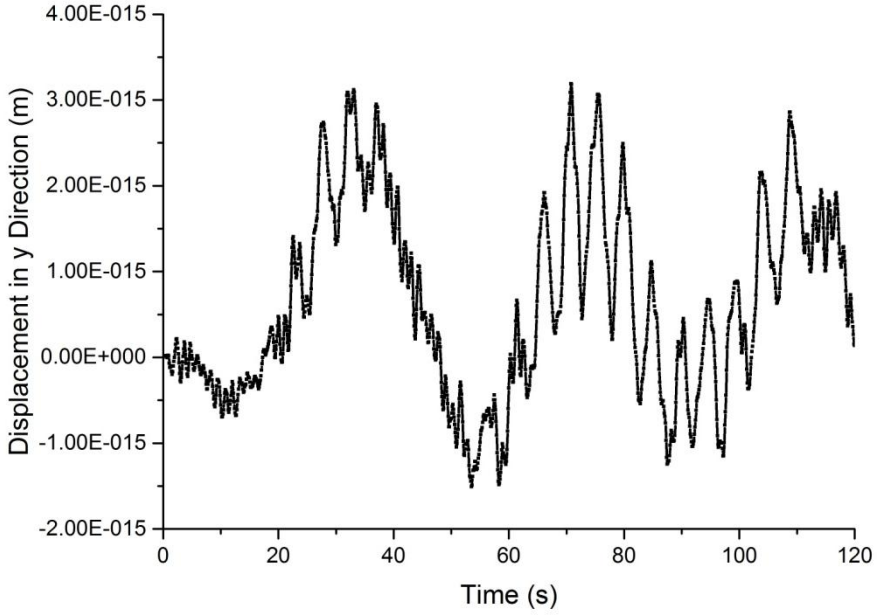

Figure 5. Displacement of Buoy's Center of Gravity in y Direction

With Orcaflex, tangential tensions at the top end of each mooring line are obtained separately, which is used for comparison with the tension results from MOORING3D code.

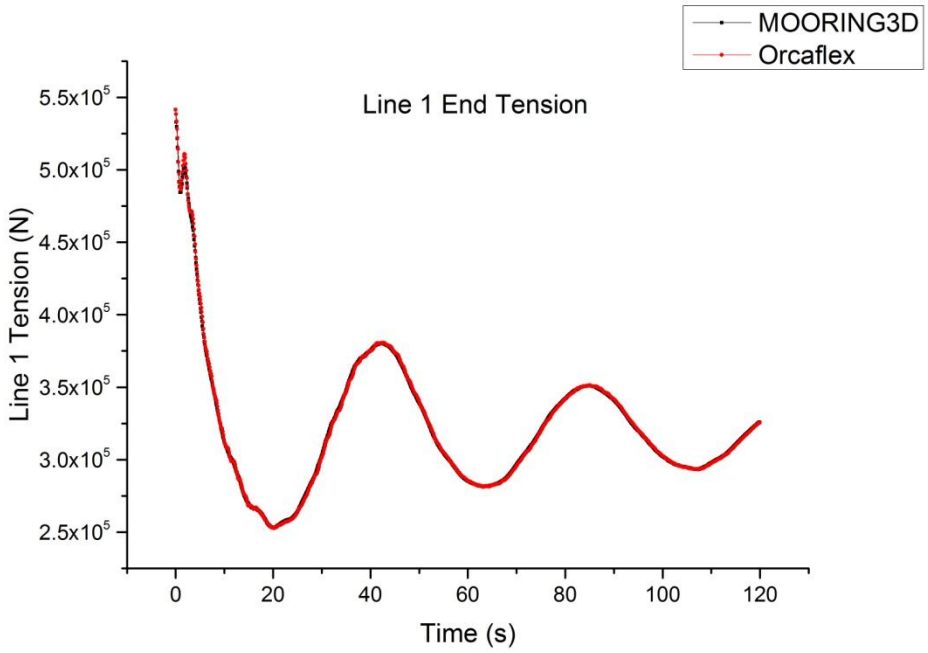

Figure 6. Line 1 Tension Comparison between MOORING3D and Orcaflex

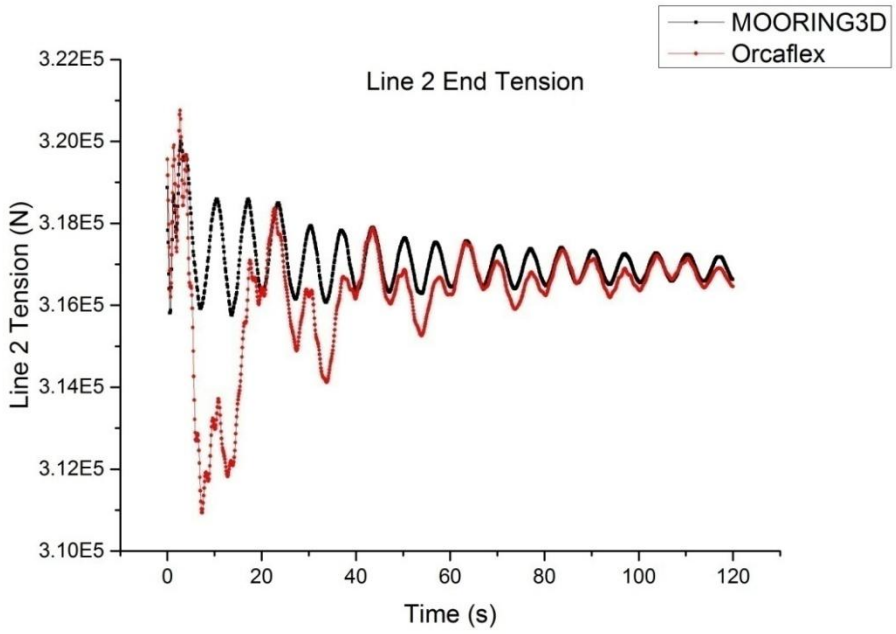

Figure 7. Line 2 Tension Comparison between MOORING3D and Orcaflex

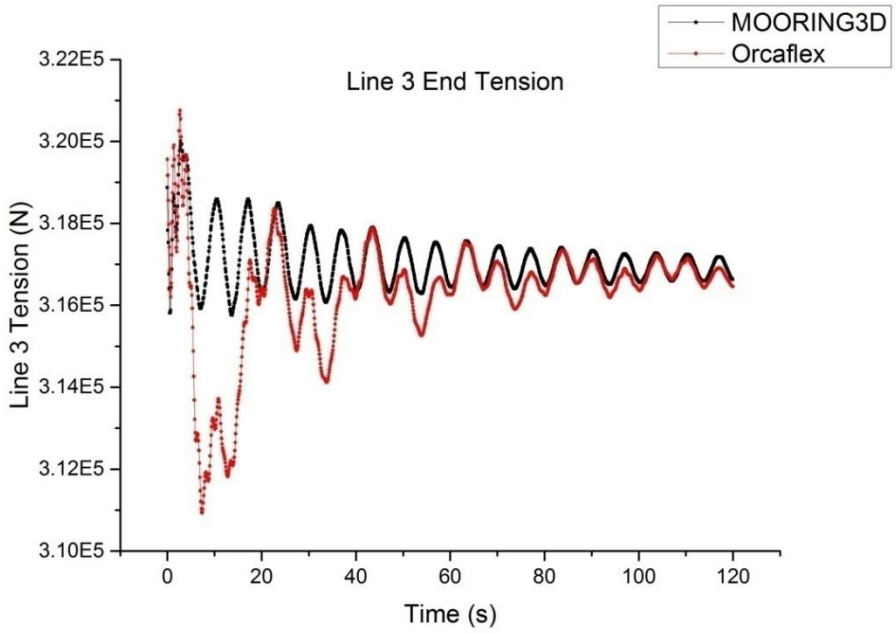

Figure 8. Line 3 Tension Comparison between MOORING3D and Orcaflex

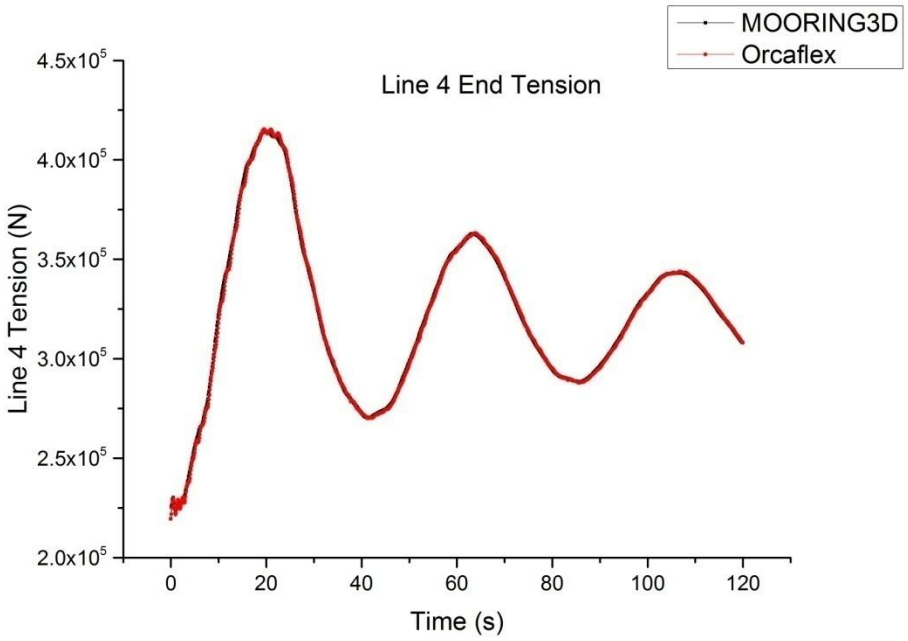

Figure 9. Line 4 Tension Comparison between MOORING3D and Orcaflex

The comparison of the cable tensions from Line 1 to Line 4 is shown in Figure 6 to Figure 9. From the figures it can be seen that for the lines in x direction, the curves of tension look very similar. While in y direction, as it's not the main direction of the free-decay motion, there exist many short-periodic oscillations in the motion, which induces differences in tensions of Line 2 and Line 3. However, compared to the value of total tension in Line 2 and Line 3, the difference between the two methods is very small. The maximum difference between the two results is only1.78% of the total tension computed in Orcaflex, which is negligible. From the test it can be seen that the MOORING3D code is able to simulate the dynamic responses of the mooring lines.

Element Number Study

To make sure that the results from MOORING3D are independent of the element number which is used to divide the mooring line model, a study of the influence of element numbers on the final results is conducted.

The element number that is used throughout the research is 35, which means each mooring line is divided into 35 segments with equal length. To demonstrate that 35 is enough to provide accurate simulation, tests with element numbers of 70 and 140 are conducted for comparison.

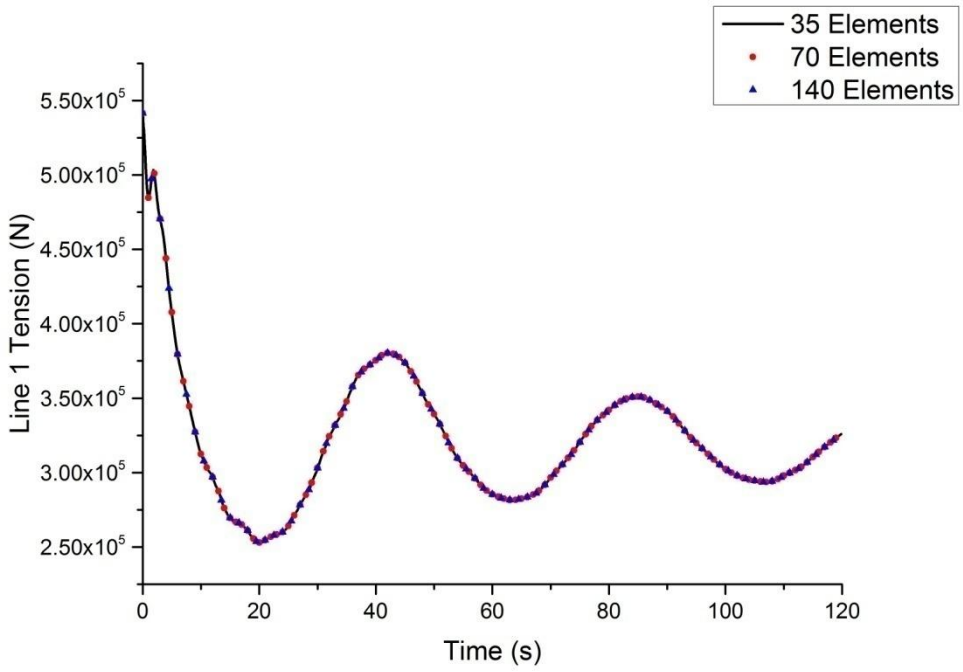

Figure 10. Line 1 Tension Comparison between Different Element Numbers

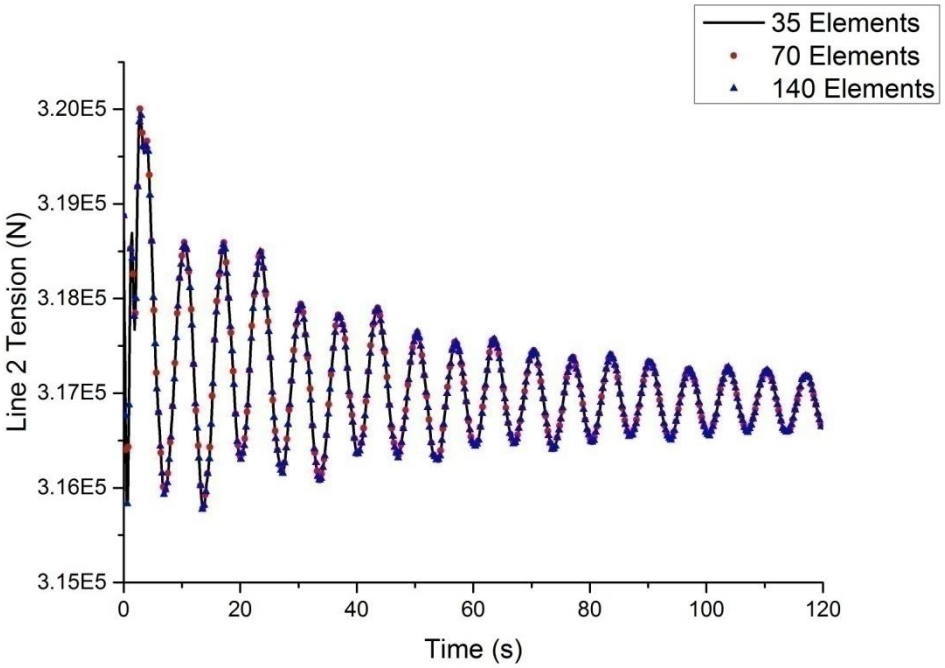

Figure 11. Line 2 Tension Comparison between Different Element Numbers

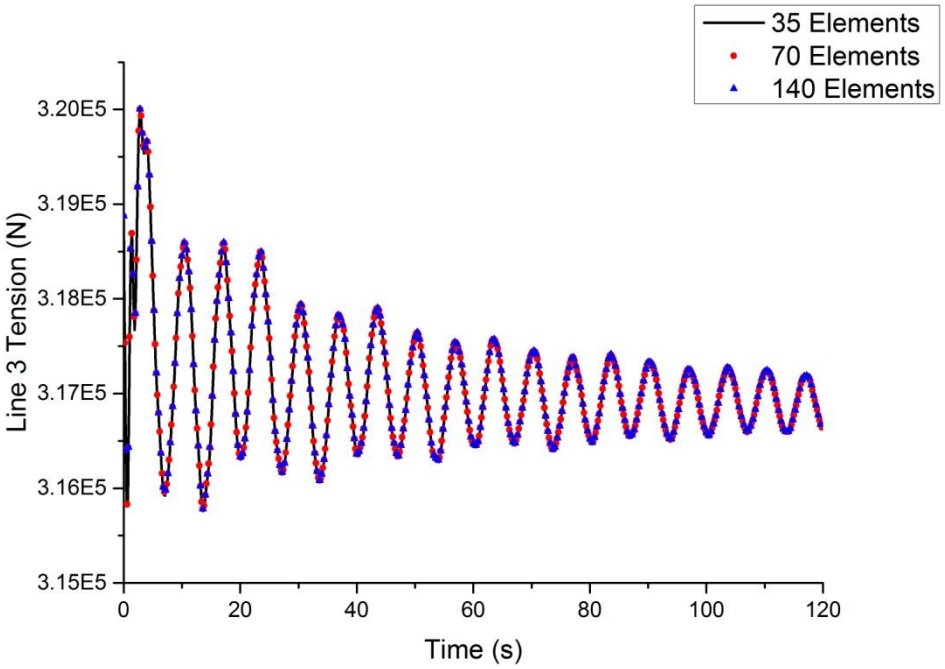

Figure 12. Line 3 Tension Comparison between Different Element Numbers

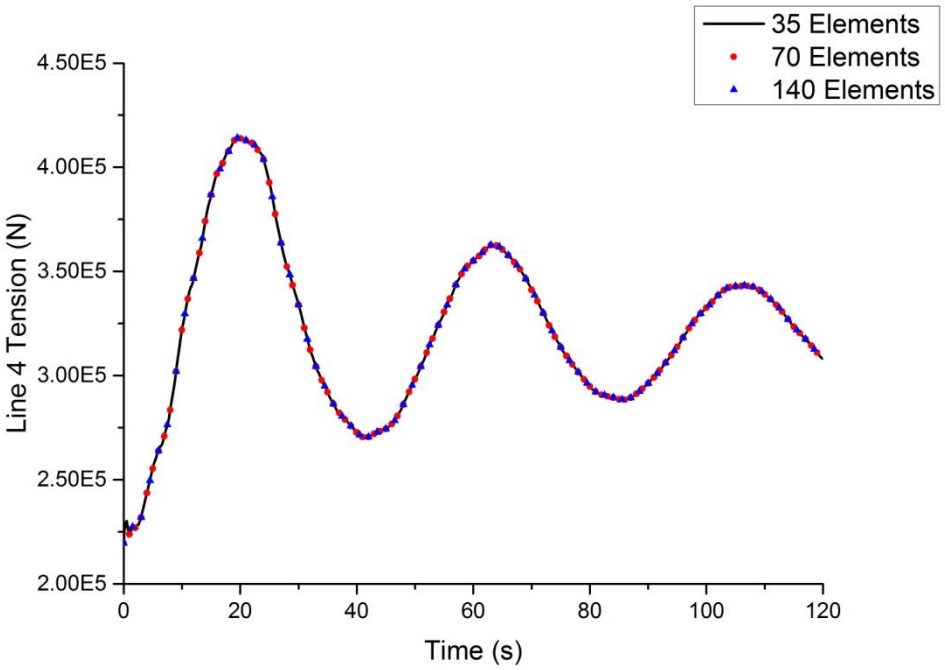

Figure 13. Line 4 Tension Comparison between Different Element Numbers

Figure 10 to Figure 13 illustrate the comparison of the cable tensions from Line 1 to Line 4 simulated with different element numbers. From the pictures it can be seen that the change of element number has almost no effect on the final results, which means that the element number of 35 selected for simulation is able to provide accurate estimation of the dynamic responses of the mooring line system.

Time Increment Study

In addition to element number, the time increment at every time step for simulation is also a variable that may cause inaccurate results. To confirm that the results we get with time equal to 0.1s are independent of time increments, two more cases with time increments equal to 0.01s and 0.2s are conducted for comparison.

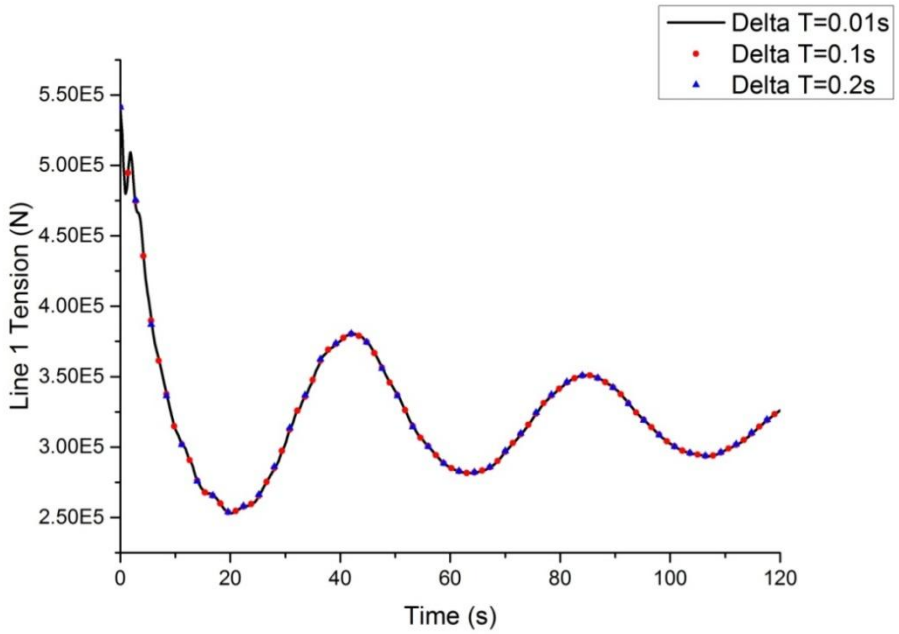

Figure 14. Line 1 Tension Comparison between Different Time Increment

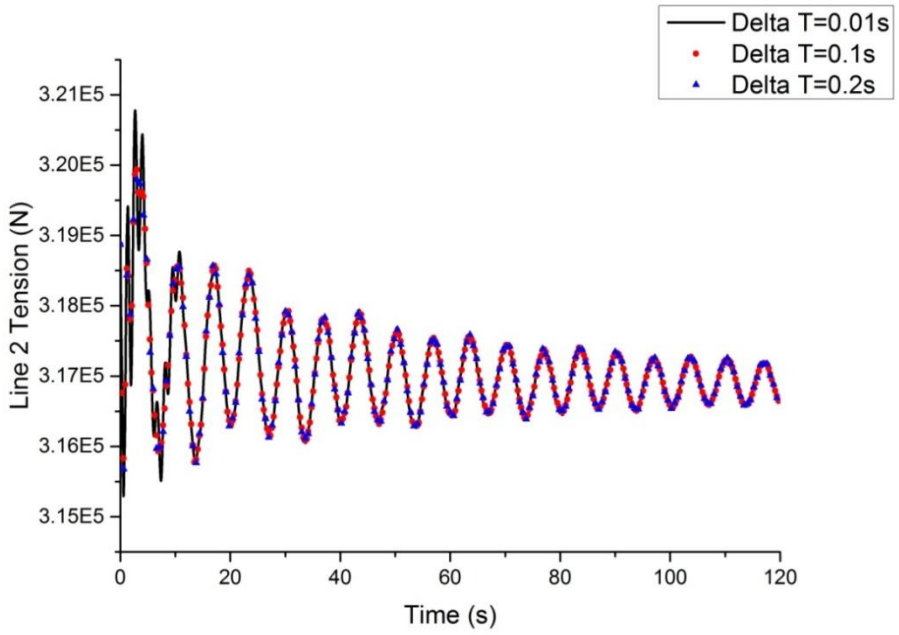

Figure 15. Line 2 Tension Comparison between Different Time Increment

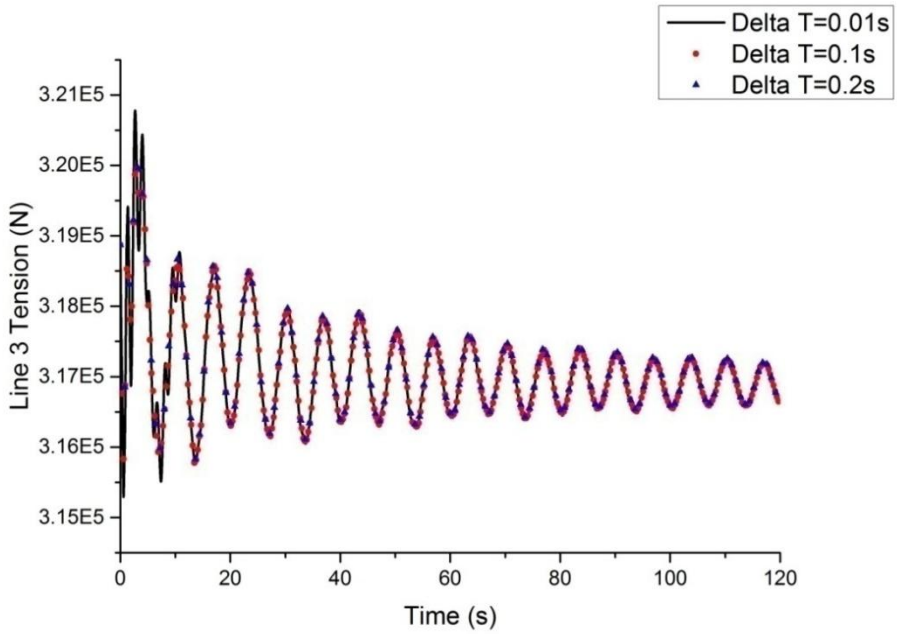

Figure 16. Line 3 Tension Comparison between Different Time Increment

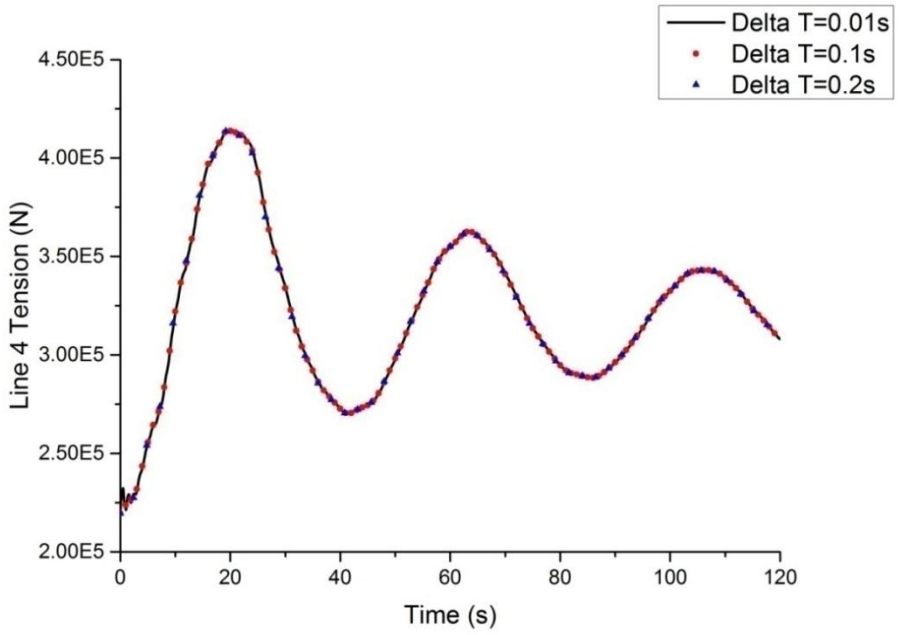

Figure 17. Line 4 Tension Comparison between Different Time Increment

By comparing the three cases in terms of cable tensions with different time increments from Figure 14 to Figure 17, it can be seen that the results don't change a lot with the change of time increment. The comparison illustrates that the cable tensions simulated by MOORING3D with time increment equal to 0.1s are accurate and reasonable, and MOORING3D is qualified for the subsequent study.

Computational Fluid Dynamics (CFD)

Background

The fluid field around the buoy is computed by unsteady incompressible three-dimensional Reynolds-Averaged Navier-Stokes (RANS) method in time domain, which is called the Finite Analytic Navier-Stokes (FANS) code(Chen et al., 2013; Chen et al., 1988, 1989; Huang et al., 2012; Pontaza et al., 2004, 2005). The fluid domain is divided into finite volume scheme to solve the continuity equation. Large eddy simulation (LES) turbulence model, which applies volume-averaging Navier-Stokes equation, is used to simulate the turbulence. Small scale vorticity is filtered out with this method to improve the computational efficiency as well as ensure the simulation quality. Eq. 14 is the differential equation used by LES method.

$$\frac{\partial \overline{u}_i}{\partial t} + \frac{\partial}{\partial x_j}\left(\overline{u_i}\,\overline{u_j}\right) = -\frac{1}{\rho}\frac{\partial \bar{p}}{\partial x_i} + \nu \frac{\partial^2 \overline{u_i}}{\partial x_i \partial x_j} - \frac{\partial \tau_{ij}}{\partial x_i} \tag{14}$$

where τ_{ij} is the subgrid stress. It is determined by Smagorinsky's subgrid-scale turbulence model shown from Eq. 15 to Eq. 20.

$$\tau_{ij} = \overline{u_i u_j} - \overline{u_i}\,\overline{u_j} \tag{15}$$

$$\tau_{ij} = -2\nu_t \overline{S_{ij}} \tag{16}$$

$$\nu_t = (C_S \Delta)^2 \sqrt{2\overline{S_{ij}\,S_{ij}}} \tag{17}$$

$$S_{ij} = \frac{1}{2}\left(\frac{\partial \overline{u}_i}{\partial x_j} + \frac{\partial \overline{u}_j}{\partial x_j}\right) \tag{18}$$

$$\Delta = \left(\Delta_x \Delta_y \Delta_z\right)^{1/3} \tag{19}$$

$$C_S = 0.1 \tag{20}$$

where $\overline{S_{ij}}$ is the local strain tensor.$C_S$is the Smagorinsky's coefficient. Δis a vorticity size value which filter out any vorticity smaller than it.

To best describe the motions of each subdomain of the fluid, an overset grid approach (Meakin, 1999)is used. Figure 18 shows what a typical overset grid is like. From the picture it can be seen that the red grid covers a common region with the blue grid. In this way, it is more flexible to simulate the relative interactions between structure and fluid without time consuming grid-regeneration process. With overset grid method, information between each two adjacent subdomains is transferred by overlapped common region between both borders. The overset grid system for the buoy is shown in Figure 19. Each block is presented with a different color.

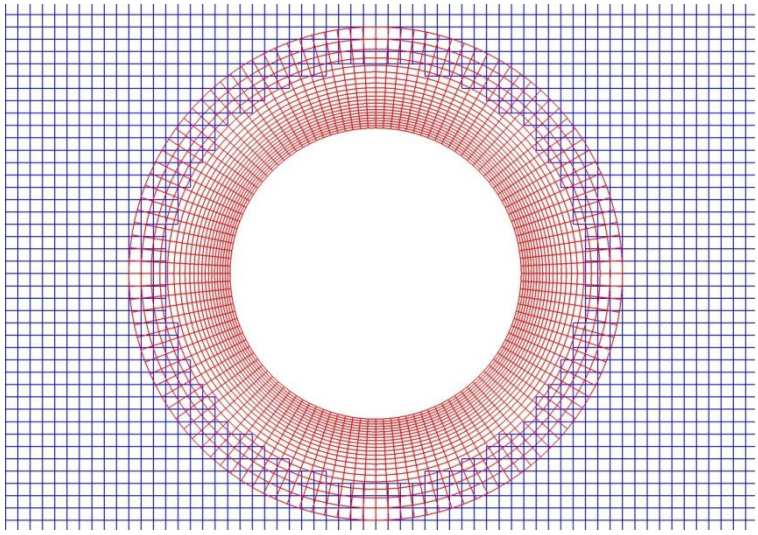

Figure 18. Overset Grid

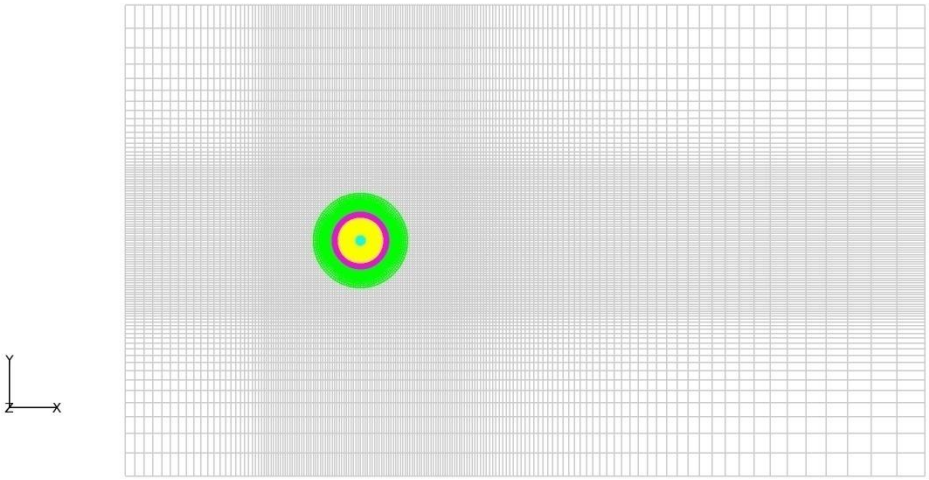

Figure 19. Plan View of Overset Grid System for Buoy

Every block stands for a calculation subdomain in the fluid. The division and meshing for each block is based on its position and characteristics. From Figure 20 it can be seen that the grid around the buoy is much finer than that in the fluid field away from

the structure, in both vertical and horizontal direction, which enables detailed resolution of the layer near the buoy and reduces the CPU computation time at the same time.

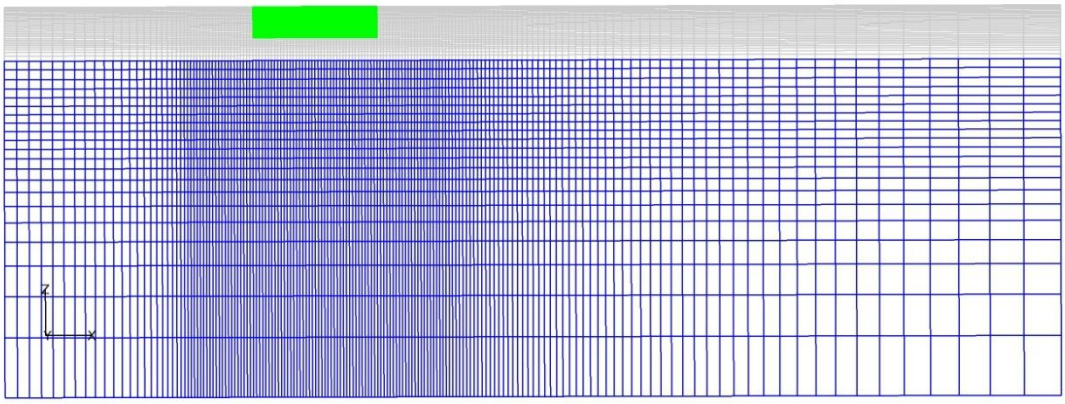

Figure 20. Side View of Overset Grid System for Buoy

Figure 21 shows the total computational fluid grid in an overview form. The whole fluid domain is set to be designed in a rectangular shape, and is divided into several blocks for calculation. The grid's parameters are normalized by the characteristic length D, which is the outer diameter of the buoy. The total fluid domain size ranges from $-5 \leq x/D \leq 12$,$-5 \leq y/D \leq 5$ and $-6.28235 \leq z/D \leq 0$. In this way, the grid is applicable for buoys with different dimensions and fluid velocities. For the global coordinate system, x axis is in the incoming flow direction, y is in the cross-flow direction, and z is pointing to the axial direction along the buoy (Figure 21).

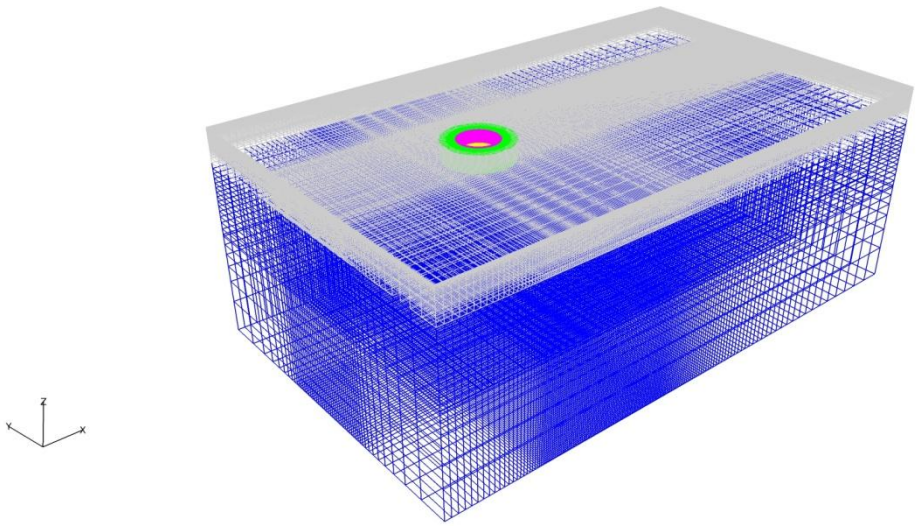

Figure 21.Overview of Fluid Domain Grid for Buoy

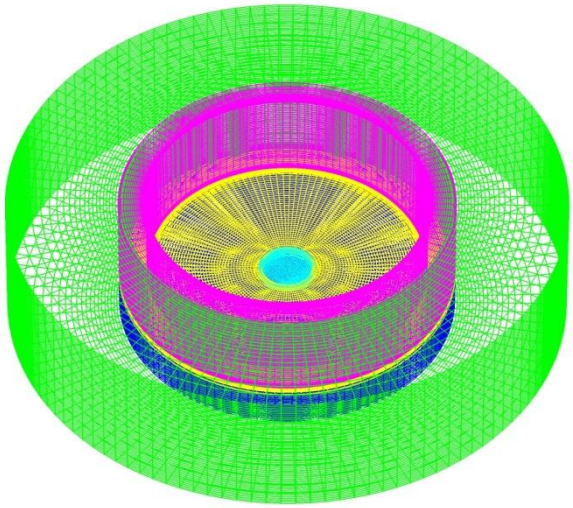

Figure 22. Detailed Fluid Grid around Buoy

There are 7computational blocks in total. For the fluid that is near to the buoy, its grids are set as concentric cylinders with different radius (Figure 22). There are 5 cylindrical columns surrounding the boundary of buoy and 2rectangular blocks

describing the farther area of the fluid. By comparing the grid density of Figure 22 and that of the rectangular blocks in Figure 21, it is obvious that the mesh size becomes coarser as the distance away from the buoy becomes larger. Block 1 is the light blue cylinder at the bottom of the buoy's center axis, whose upper face stands for part of the bottom surface of the buoy. The dimensions of Block 1 is $31 * 31 * 27$. Block 2 is the yellow hollow cylinder with dimensions of $69 * 122 * 11$. Block 2 shares the same upper face level with Block 1. These two blocks constitute the bottom surface of the buoy with overset grid on the boundary between each other (Figure 23). The reason why it needs two blocks to make up one bottom surface is that a center surface must be established additionally to prevent centripetal grid lines in Block 2 converge to a singular point and influence the quality of the solution. From Figure 23 it can be seen that Block 1 and 2 use different types of meshing on their upper surfaces to prevent the problem.

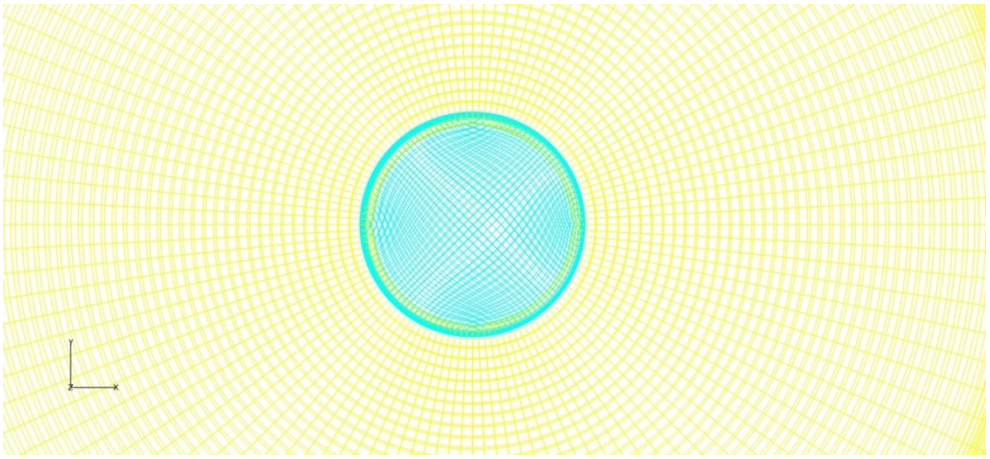

Figure 23. Over View of Upper Surface in Block 1 and Block 2

Block 3 is the magenta hollow tube cylinder standing on top of the second block. The inner boundary of the cylinder represents the outer boundary of the buoy model. Block 3 has the dimensions of $122 * 21 * 48$. It's outer diameter is the same as the outer diameter of Block 2. These two blocks have overset grid for information transfer in vertical direction. Block 4, which is the dark blue hollow cylinder, has the same outer diameter as Block 3 and same inner diameter as Block 2. The identical diameters make sure that Block 4 can transfer information with inner cylinder Block 1 and with upper cylinder Block 2. With dimensions of $122 * 22 * 61$, the centripetal-direction grid line is evenly laid around the diameter of the cylinder, which is uniform with Block 2 and Block 3.

Blocks 1 to 4 represent the fluid area which is near to the buoy model. These four blocks are connected with each other with overlapped grid. Blocks 2,3,4 have the same outer diameter which provides an integral cylindrical surface to communicate with outer tube cylinder Block 5. As for Block 5, it works as a transition area to transform the block geometry from cylinder to rectangle as well as enlarge the grid size from center to border gradually.

The Block 5 is connected to outer fluid area Block 6, with grey color in Figure 21. From Figure 24 it can be seen what Block 5 and Block 6 is overlapped with each other. The grid sizes of Block 6 and Block 5 in the common region has kept similar, so that a more accurate interpolation can be done while exchanging information between the two blocks. The dimensions of Block 6 are $165 * 101 * 31$.

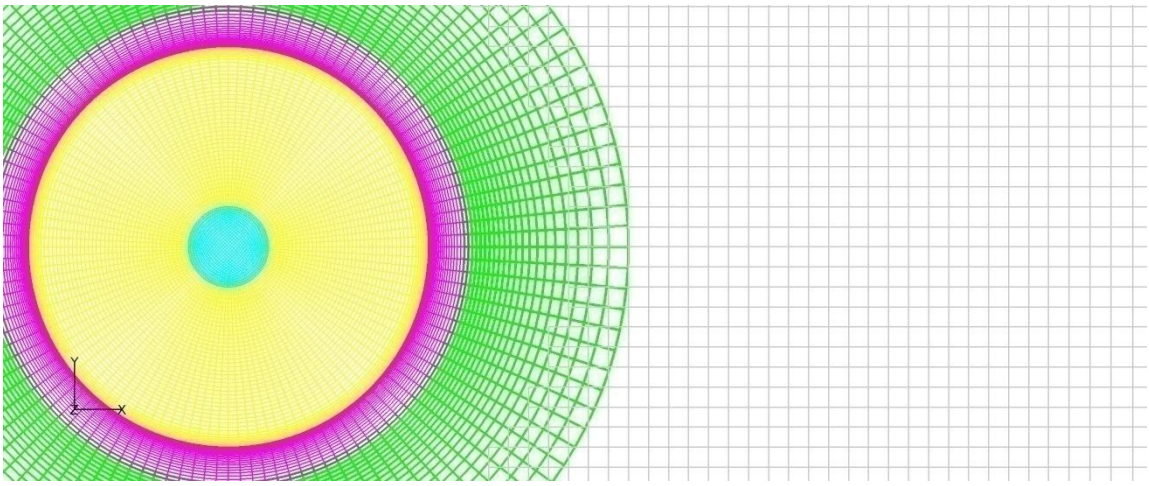

Figure 24. Upper Surface of Block 5 and Block 7

As for Block 7 with dimensions of $165 * 51 * 22$, itstands for the fluid domains that are located far from buoy model. It contains great volume of the deep water, and has an equivalent length and width as that of Block6. As Block 7 is mainly used for extend the simulation domain size and its position is far from the targeted model, the grid in it can be coarser than all other blocks.

Each block is connected to the neighboring blocks with the help of overset grid, which enables the integrity of total domain, and saves the cost of model motion calculation at the same time.

Verification

To check whether the FANS code is able to provide reasonable result, a fixed buoy case is simulated for verification. The size of the buoy follows the parameters of the buoy model used in Canada Offshore Engineering Basin at the Institute for Marine Dynamics (Ryu et al., 2006). The parameters of the prototype buoy are listed in Table2.

Table 2. Full-size Buoy Parameters

Parameter	Unit	Value
Model Test Scale		35.6
Water Depth	m	106.8
Buoy Hull Diameter	m	17.0
Buoy Height	m	7.65
Draft	m	5.65
Weight in Air	ton	878.6
KG	m	3.4
Buoy Total R_{xx}	m	4.39
Buoy Total R_{yy}	m	4.39

To facilitate a direct comparison with the model test data, numerical simulations were performed for the model scale CALM buoy system. The scale ratio for the length of model test is $\lambda = \frac{L_F}{L_M} = 35.6$. As the model test in the wave basin follows the Froude similarity scaling law ($\frac{{U_M}^2}{gL_M} = \frac{{U_F}^2}{gL_F} = {F_n}^2$) to ensure the gravity forces are correctly scaled, the corresponding scale ratio for the velocity becomes $\frac{U_F}{U_M} = \sqrt{\lambda} = \sqrt{35.6}$, and the time in the simulation will also be scaled as a ratio of $\frac{T_F}{T_M} = \sqrt{\lambda} = \sqrt{35.6}$. Besides, to make the module more applicable to models with different parameters, all the parameters in the FANS code are initialized to dimensionless number, with the characteristic length and characteristic velocity. Here we take the outer diameter of the model buoy $charl = \frac{17}{35.6}m$ as the characteristic length, and velocity in the model test $\frac{1}{\sqrt{35.6}}m/s$ as

characteristic velocity. In this way, the diameter of the buoy will become $D = \frac{D}{\lambda * charl} = 1$. Based on the model test size, the Reynolds number for the simulation is 7.14e4.

According to the result from (Ryu et al., 2006), there is little differences in the surge motion when comparing the buoy with and without a skirt. Due to the limitation of research period, only a 2D horizontal motion (surge, sway and yaw) is considered throughout the study. As no vertical motion like heave is taken into account, and the effect of skirt is very small, we simplify the buoy model to a cylinder without the surrounding skirt structure (Figure 25).

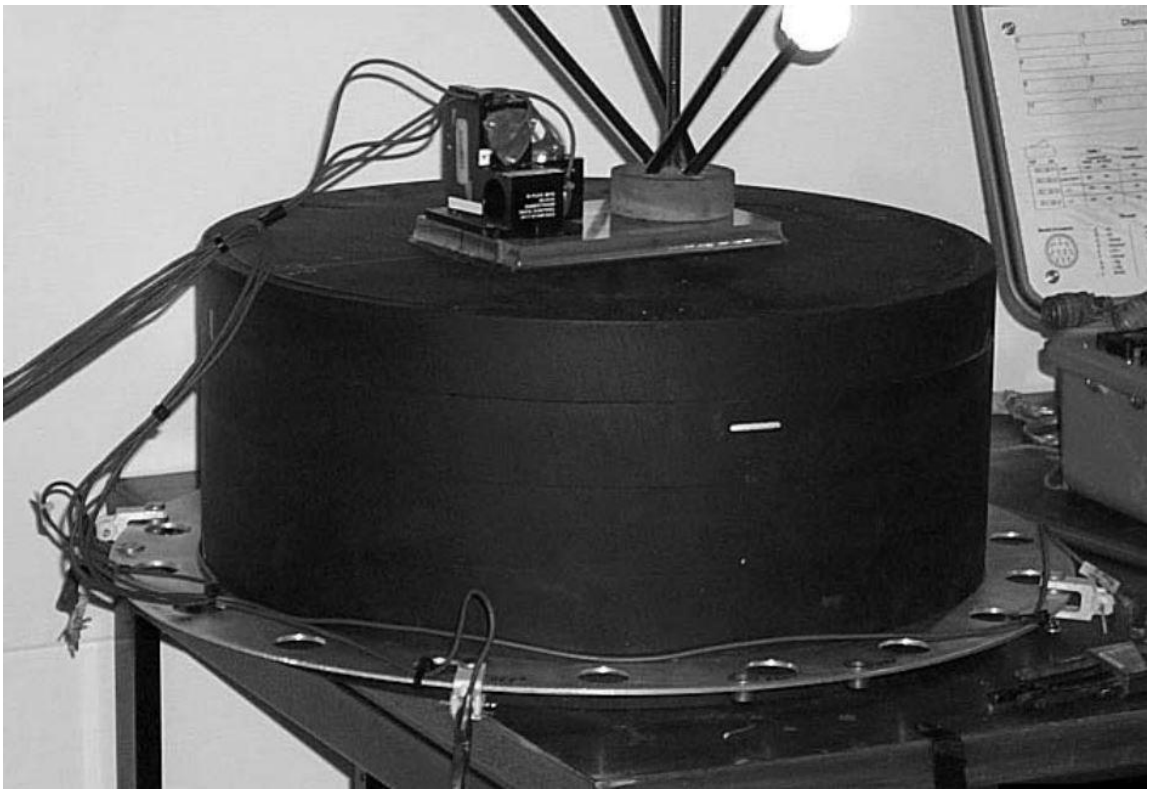

Figure 25. Buoy and Its Skirt Used for Model Test

The buoy's center of gravity is fixed at the point of (0,0) on the x-y plane. There is a current with a constant velocity of $1\,m/s$ in full size scale. The current starts from$x = -5$, which is the inlet boundary of the fluid domain (Figure 26). The current is also constant in vertical direction on the inlet surface.

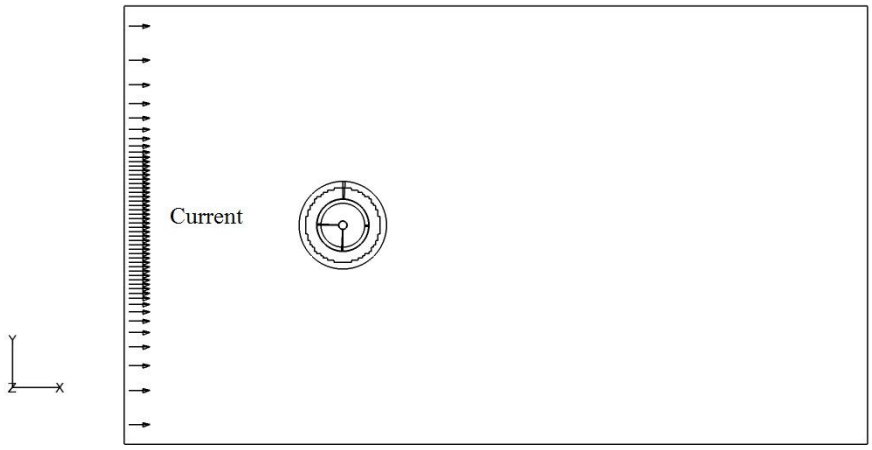

Figure 26. Current Direction for Fixed Case

Boundary condition needs to be defined for every surface of each block. For the faces constituting the boundary of the buoy model, which include the upper surface of Block 1 and 2, and inner surface of Block 3,the boundary condition of the velocity in three directions is set as moving or as prescribed boundary condition. The pressure and turbulence conditions are set to be Neumann boundary condition.

For the surfaces that stand for the uppermost surface of the fluid domain, a Neumann boundary condition is set for velocity in x and y directions, pressure and turbulence except for the velocity in z direction. As free surface's vertical motion is not

considered under the effect of current in this study, the velocity vertical to x-y plane is given by the Dirichlet boundary condition. The uppermost surface of the fluid domain is composed of the uppermost surfaces of Block 3, 5, 6. The same method of setting boundary condition is used for the other boundaries of the fluid domain. For the boundary at $y/D = 5$ and -5, the velocity in y direction is set to have Dirichlet boundary condition, while the other parameters are defined with Neumann boundary condition.

As the current direction is in x direction, the surface at $x/D = -5$ is defined as the inlet of the fluid flow. The velocity in this surface is defined in the input file, so that a prescribed boundary condition is required for the velocity parameters on this surface. For the surface at $x/D = 12$, as it's the outlet of the current, the velocities in three directions are defined as parabolic boundary conditions with the current moves continuously across the downstream boundary. Same situation works for the bottom surface of Block 7, which is also the bottom of the total fluid domain. And for other boundaries that don't belong to physical boundaries, which are only used for blocks division, they are set as interior boundary condition to eliminate any redundant physical effect on them.

The calculation time step is set to be 10000, with a time increment of 0.02, which is 0.34s for the full size scale. The total simulation time in prototype scale is 3400s, which is equal to 0.95 hour. Figure 27 and Figure 28 show the hydrodynamic forces exerted on the buoy in x and y directions separately. The data in the figures is dimensionless. From Figure 27, it can be seen that the hydro-force in x direction

oscillates greatly around a positive y axis during the first stage. Then the amplitude of oscillation begins to decay until the fluid load vibrates in a small range around the positive y axis. The result is reasonable because for the first stage, when the fluid is passing by the buoy, the dynamic condition is not stable and the load on the buoy changes greatly. After the fluid fully develops, the hydro-force on the buoy reaches a relatively stable status. But due to the alternative shedding of vorticity in the downstream direction of the buoy, the hydro-force cannot be a constant value.

It is the same reason for the oscillations of hydro-force in y direction. Although there is no direct hit from the current in y direction, the alternatively changing vortices brings small imbalance in the hydro-force on the buoy in cross-flow direction. Compared to the hydro-force in x direction, the force in y direction exhibits small amplitude oscillations, which corresponds to the behavior of vortex shedding shown in the figures below.

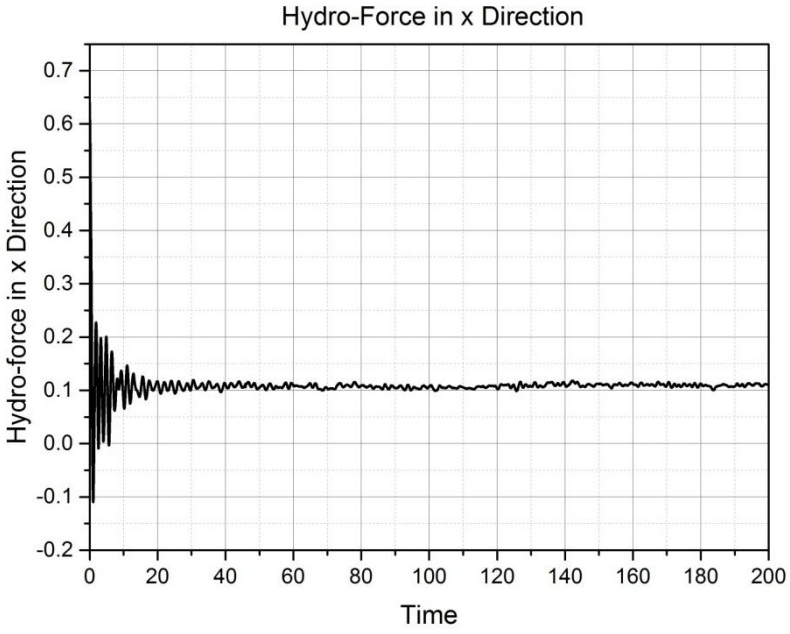

Figure 27. Hydro Force in x Direction

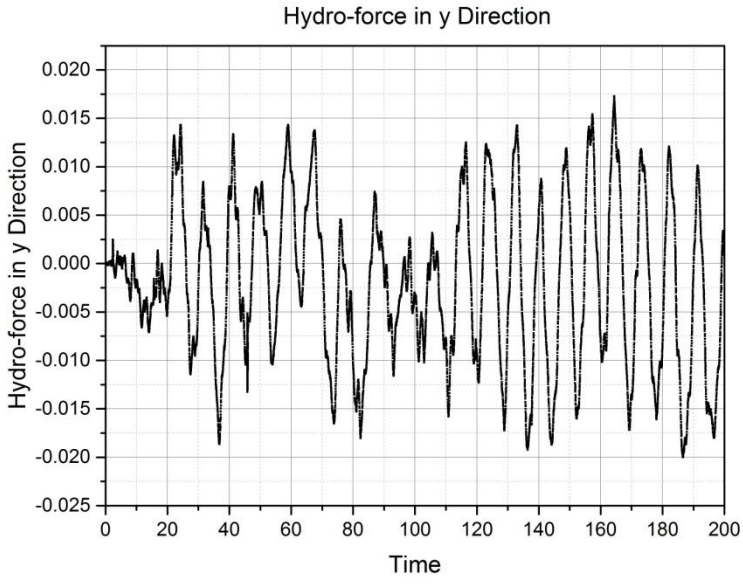

Figure 28. Hydro Force in y Direction

Figure 29 to Figure 32 are the vorticity patterns at dimensionless time 5.6, 20, 140 and 160, which refers to 95.2s, 340s, 2380s and 2720s in the full scale. The depth of the plane is -1.7m below the free surface. From the pictures the gradual evolution of the vorticity in z direction can be seen. At time=5.6, the vorticity pattern in axial direction is symmetric in the downstream side of the buoy. Compared with the following figures at further time steps, the vortices haven't been fully developed. That is why the hydro-force in x direction oscillates fiercely during the first 10 dimensionless time period and the hydro-force in y direction is relatively small. At time=20, which is the turning point where the vortices are close to fully developed and no longer symmetric. The hydro-force in inline direction turns into a relatively stable state with small oscillations. The hydro-force in cross-flow direction starts to have drastic vibration instead due to vortices' asymmetry. Figure 31 and figure 32 display the vortex pattern which is fully developed. From these two pictures it can be seen that vortex shedding has been generated. And the vorticity in each direction dominates each other alternatively as time goes by.

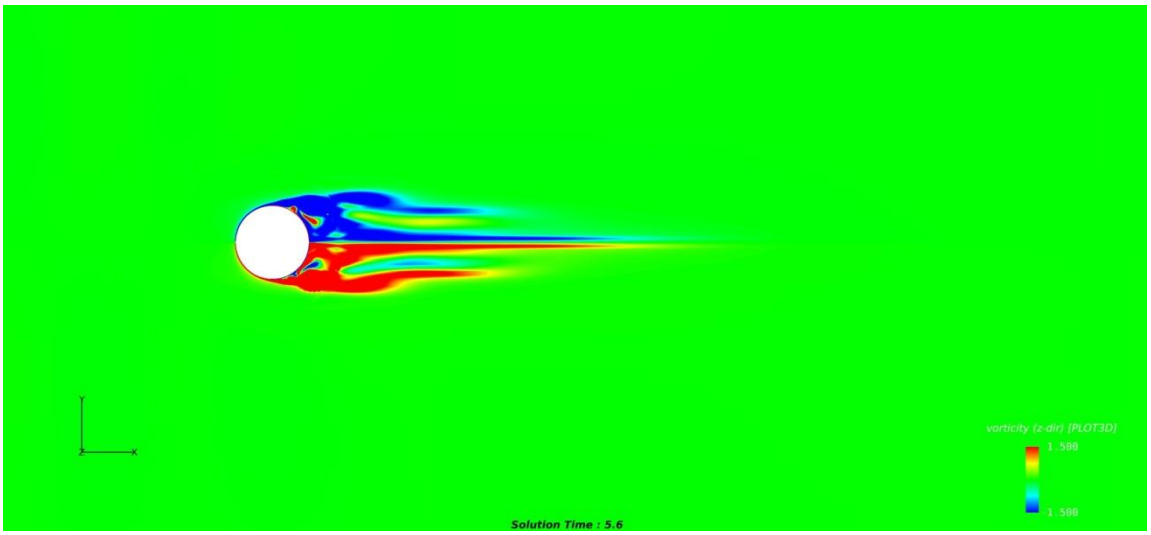

Figure 29. Vorticity Patterns in Axial Direction at Time=2.6

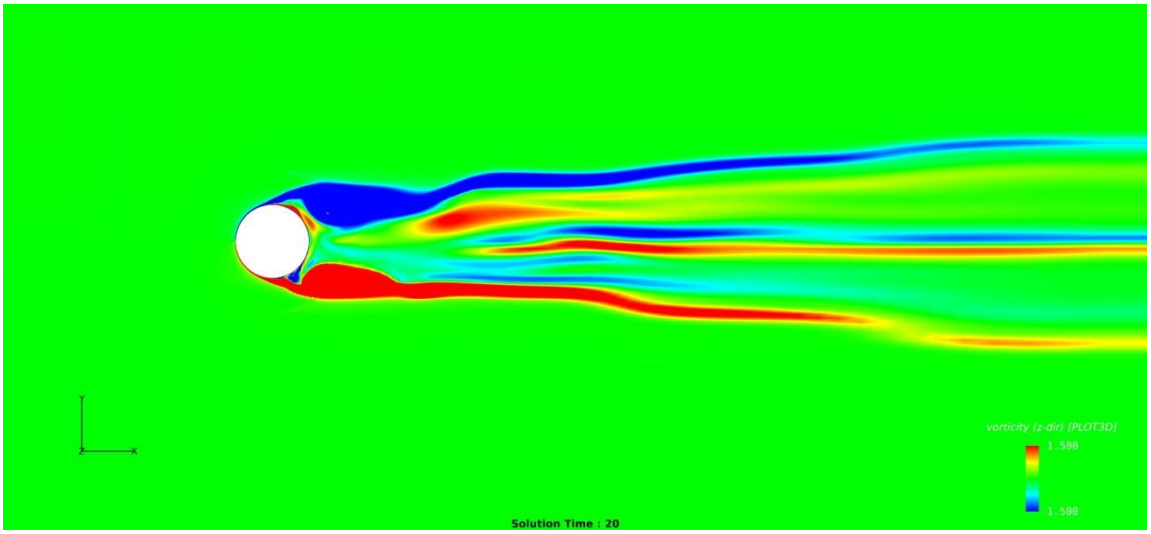

Figure 30. Vorticity Pattern in Axial Direction at Time=10

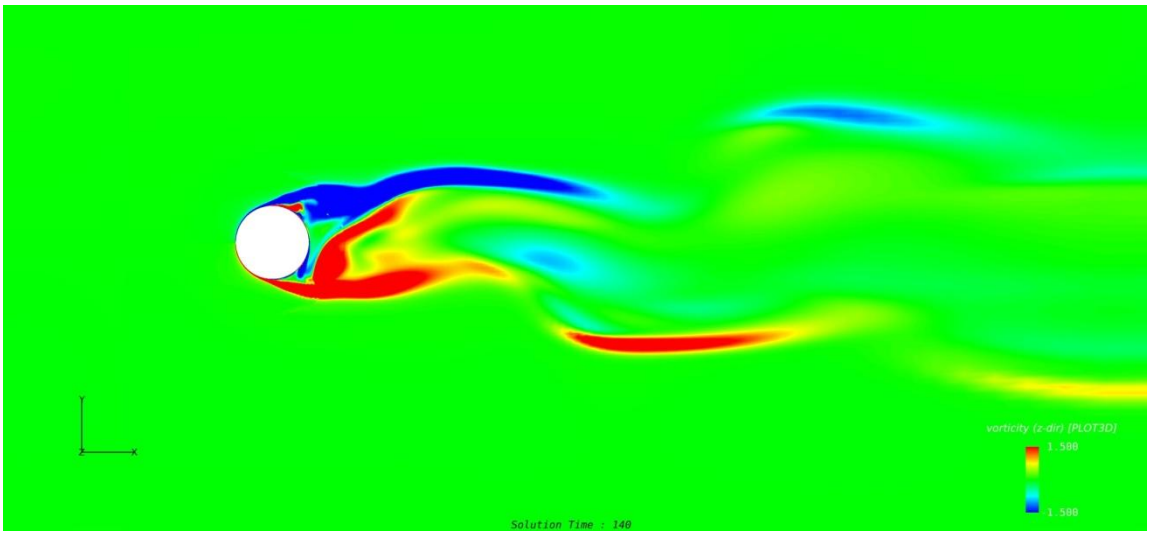

Figure 31. Vorticity Pattern in Axial Direction at Time=17.2

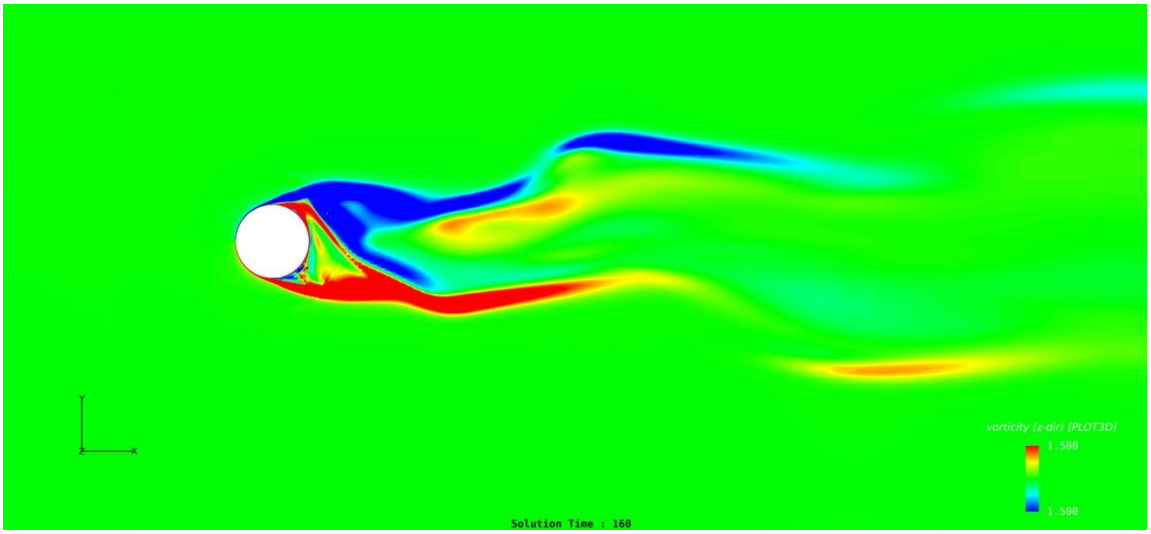

Figure 32. Vorticity Pattern in Axial Direction at Time=29.2

Figures 33, 34 and 35 depict the 3-dimensional hydro-force pattern at solution time 5.6, 140 and 160. The direction of observation is from –x to +x. From Figure 33 it can be seen that when the vortex is symmetric at the beginning, the forces exerted on the

buoy is also symmetric. As the upstream side of the buoy faces the current directly, there exists one stagnation area on the surface where the hydro-force is the strongest. Figures 34 and 35 illustrate the change in the hydro-force when the vortex is shedding. By comparing the two pictures it can be seen that the hydro-force in y direction changes a lot due to the vortex shedding, which also confirms the drastic change in Figure 28.

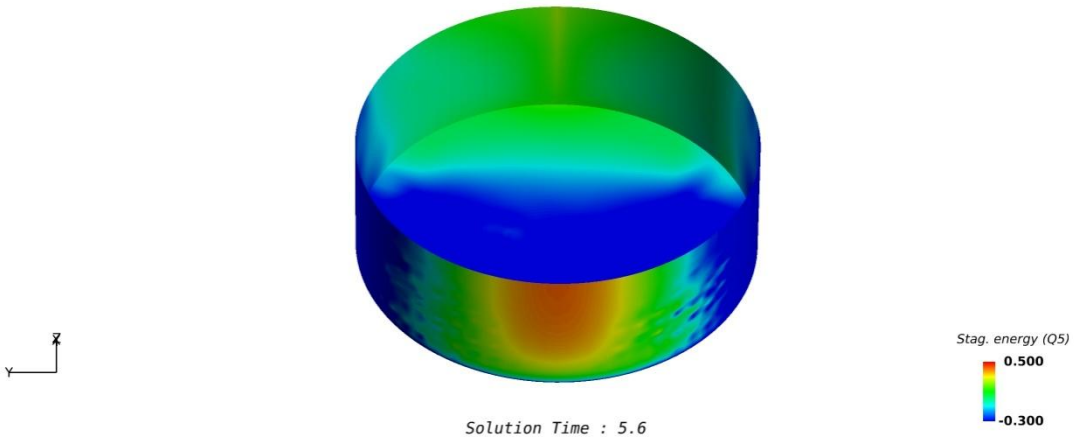

Figure 33. Hydro-force Pattern at Time=5.6

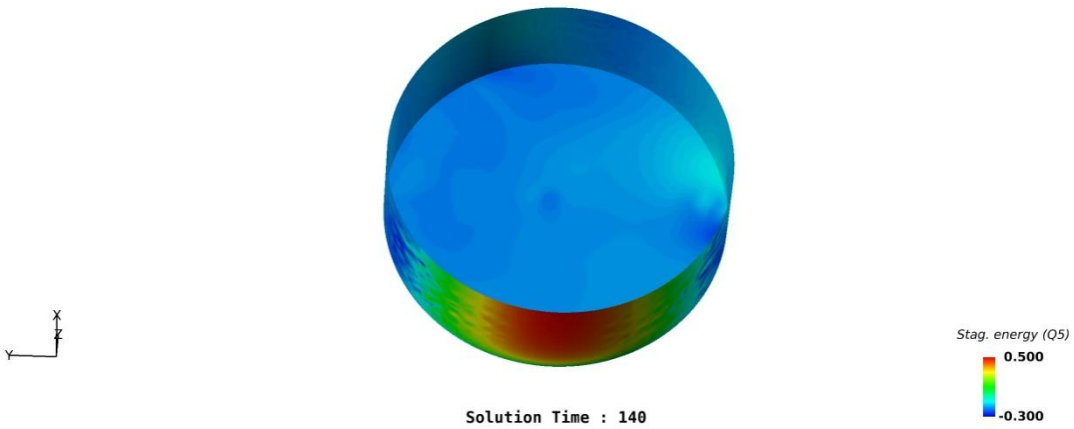

Figure 34. Hydro-force Pattern at Time=140

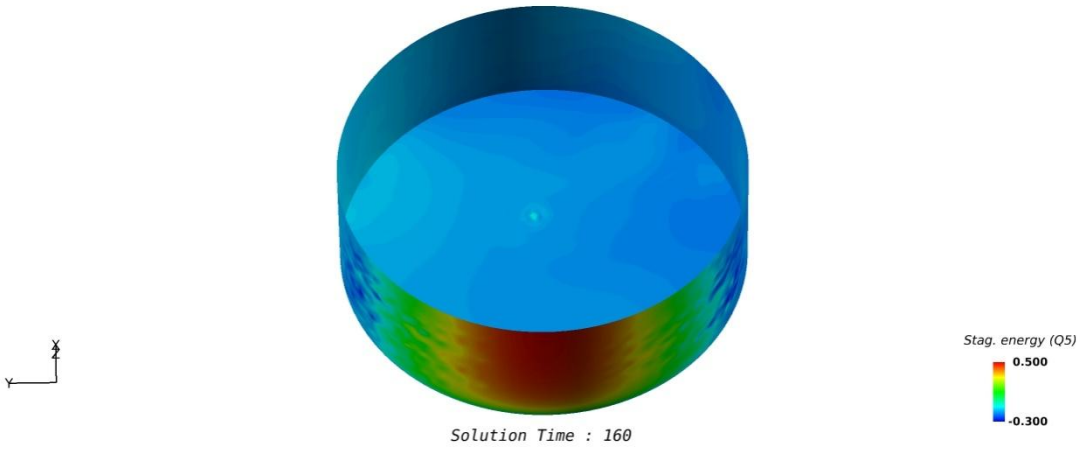

Figure 35. Hydro-force Pattern at Time=160

Figures36,37 and 38 display the vorticity in y direction and velocity on the fluid plane in axial direction. Each arrow stands for the velocity magnitude and direction at the local point. The color illustrates the vortex magnitude. From the pictures it can be seen that there also exists fluidic interaction in vertical direction throughout the process. The vorticity under the bottom of the buoy and downstream side of the buoy is especially obvious.

By comparing Figure 36 and Figure 37 it can be seen that compared to the vortex pattern in other areas, such as y=-0.1, the vortex in y direction on the center plane of the buoy's symmetry in streamwise direction, which is y=0, and is more complicated because it is located on the interface between the two domains divided by the central streamwise line. By comparing the patterns in Figure 36 and Figure 38 at y=0, it can be inferred that as the vortex develops, the contour of the vortex in y direction transforms

from narrow strip shape to circular shape. And the vortex below the bottom of the buoy is more evenly distributed when the fluid is fully developed.

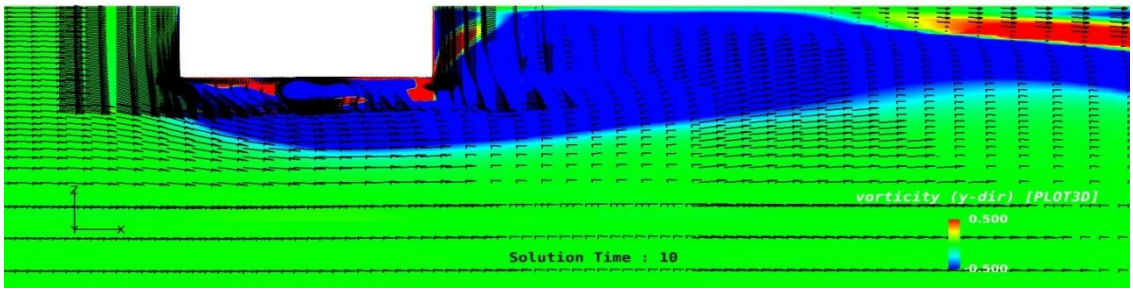

Figure 36. Velocity and Vorticity Pattern at (y=0, T=10)

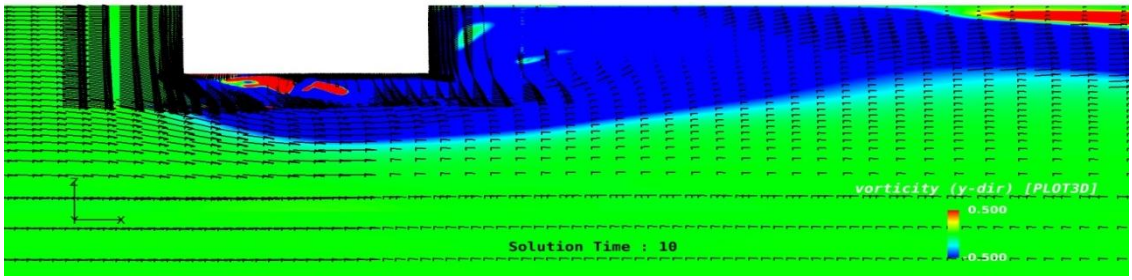

Figure 37. Velocity and Vorticity Pattern at (y=-0.1, T=10)

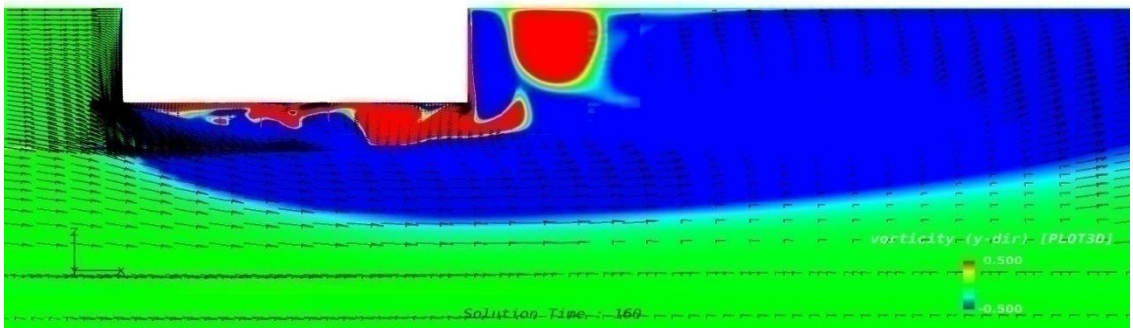

Figure 38. Velocity and Vorticity Pattern at (y=0, T=160)

From the analysis above, it can be seen that the FANS code is able to simulate the fluid domain with a reasonable and clear result, which means it can be applied for the further research.

Interface Module

The aim of this study is to provide a new simulation method to analyze the dynamic response of CALM buoy systems. From the previous introduction, we are able to calculate the hydrodynamic behaviors of both buoy and cables. The interface module serves as a transmission channel delivering the essential information to the FANS module and MOORING3D module. The general function and procedure for the whole simulation is demonstrated in Figure 39. The FANS code would first calculate the fluid dynamic behavior including hydro forces on the buoy and fluid velocity at the beginning of each time step. The calculation is based on the updated information obtained from last time step, including the position of the buoy and the velocity and vorticity of the fluid. With the newly obtained hydro forces, the total forces acting on the buoy can be calculated by combining the hydro forces together with the mooring lines' tensions. With the help of motion module, the new displacement of the buoy is calculated with the new total forces. Being attached to the fairlead points on the buoy, the mooring lines are forced to move with their top-end elements moving together with the buoy. The new displacement of the buoy's fairleads will induce motions to the mooring lines, which

will generate new tensions and moments as external forces and moments on the buoy from the cables.

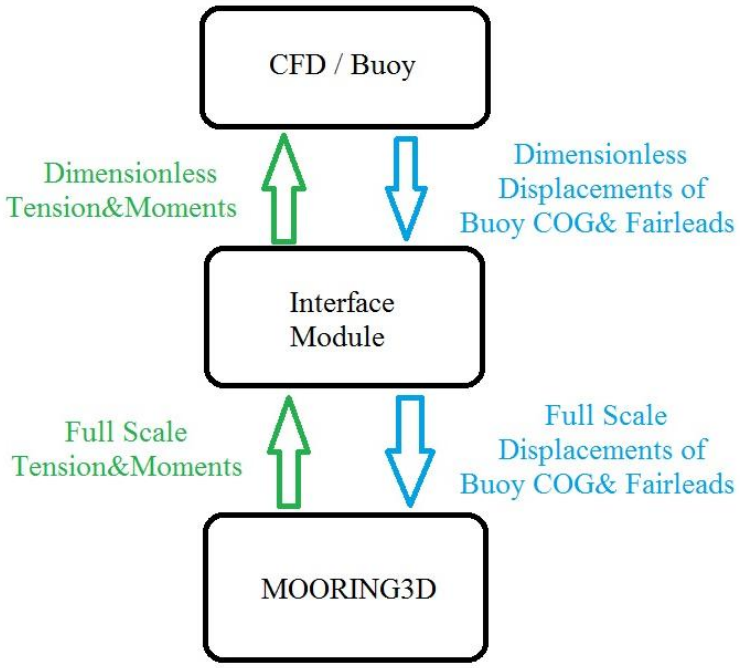

Figure 39. Interaction between Three Modules

In the coupled FANS/MOORING3D simulations, the interface module is responsible for transferring the buoy's updated displacement to the MOORING3D module as an input, and transferring the tensions and moments caused by the new displacement back to the FANS code as an external effect on the buoy. As all the parameters in the main code (FANS code) are dimensionless, while the parameters used in MOORING3D code are dimensional, it is necessary to normalize the input for the

MOORING3D code and dimensionalizing the input for the FANS code. Besides, compared to the model test scale simulation conducted in FANS code, the MOORING3D code uses a prototype scale simulation. The scaling down and scaling up procedures also need to be taken into account in the interface module.

After considering scaling laws and normalization, the inputs for FANS and MOORING3D modules will be deformed like:

For the displacement of buoy,

$$x_{cable} = x_{buoy} * \lambda * charl \tag{21}$$

for the total tension and moment of mooring line,

$$T_{buoy} = \frac{T_{cable}}{\rho * charl^2 * charu^2 * \lambda^3 * 1.025} \tag{22}$$

$$M_{buoy} = \frac{M_{cable}}{\rho * charl^3 * charu^2 * \lambda^4 * 1.025} \tag{23}$$

for the time increment,

$$tau_{buoy} = \frac{tau_{cable}}{\sqrt{\lambda} * charl} * charu \tag{24}$$

where x_{cable} , T_{cable} , M_{cable} , tau_{cable} stand for parameters in MOORING3D module, and x_{buoy} , T_{buoy} , M_{buoy} ,tau_{buoy} stand for parameters in FANS module. $\lambda$is the length scale ratio from full size to model scale. $charl$and$charu$ are characteristic length and velocity used for normalization in FANS code.

CHAPTER III

FREE-DECAY TEST FOR CALIBRATION

The aim of this research is to provide a new simulation method to predict the dynamic response of CALM buoy systems. With further development in the future, it may also be used as a tool for the motion analysis of various types of floating production systems. After the coupled code is established in Chapter I, the next step is to calibrate the model of CALM buoy system for further prediction of its hydrodynamic responses.

Experiment Background

Many model experiments have been conducted during the past study, among which the free-decay test is a widely-used way to analyze the hydrodynamic characteristics of the CALM system (Duggal et al., 2005; Salem et al., 2012; Woodburn et al., 2005), including the natural period of the buoy's for the surge motion. To calibrate the dynamic characteristics of the CALM buoy system established by the coupled code, a free-decay test is first conducted. A test with the same parameters of the model and environmental conditions is also conducted with commercial software Orcaflex. The results from the model test, coupled code and Orcaflex will be compared together to verify whether the model established in coupled code has the same characteristics with the one in model test.

In the present simulation, only the model tests in wave basin are considered. Simulation in full scale will require finer grid resolution and more computer resources. Based on this principle, the free-decay model test conducted in the Offshore Engineering Basin at the Institute for Marin Dynamics in Canada (Ryu et al., 2006) will be replicated with the coupled code and Orcaflex separately.

Although simulating model-scale tests will provide a better resolution for the FANS part, there also exist some limitations in the simulation of mooring system. To conduct the model experiment in the wave basin, scaling law of Froude similarity is used to scale down the parameters from full-scale size to model-scale size. However, due to the limitation of experimental facility, including limited water depth and characteristics of experimental materials, most of the model mooring lines can hardly be "directly" scaled. In most cases, truncated mooring method is used to simulate equivalent dynamic behaviors with mooring line length and other characteristics disobeying the Froude scaling law. Like the model mooring lines' parameters in Table 3. Pretension is exerted on the initial state of the mooring lines to add additional load onto the buoy. In this way the model is able to reach the desired draft and fairlead angle which are 5.65 m and 45 degrees in the full-scale condition. From Table 3 it can be seen that the total length of mooring line is shortened and a large pretension is enforced, which means the lines no longer have the characteristics of slender rods. If the mooring line models are not slender rods, it is infeasible to use MOORING3D code for simulation.

Table 3. Original Mooring Lines' Parameters for Model Test in the Paper

	Unit	Mooring
Length	m	133.3
Wet Weight	kg/m	3
Diameter	mm	NS
EA	metric tons	1963
Pretension	metric tons	150

To fulfill both requirements for the buoy part and mooring lines part, we first need to set up a CALM buoy system model with the scaled-size buoy in the model test (Ryu et al., 2006) and a mooring line system with modified parameters applicable for MOORING3D to simulate. The parameters of the buoy are shown in Table 2. For the catenary mooring line model, a parameter study is used to get an appropriate set of parameters which is able to generate a similar hydrodynamic response to the full-scale buoy in the free-decay test. If the behavior of the new CALM buoy system in the free-decay test is similar to the behavior of the CALM buoy model in the model test, the CALM buoy system in the coupled code is calibrated well. It can be used for prediction under other sea states in the next study.

Experiment Set-up

Buoy Part

As for the FANS code to simulate the model of the buoy, the parameters of the model are the same as the one used in the model test. Method of scaling down the parameters and normalization are also the same as the method mentioned previously in Chapter I. The overview of the computational fluid domain is the same as Figure 21. However, different from the previous fixed buoy model case, the CALM buoy in the free-decay test will move under the effect of fluid and mooring lines in static water. Considering the buoy can be regarded as a rigid body in the ocean, it is convenient to set all the blocks as an uniform fluid domain and move all grid blocks simultaneously.

A motion module is established to calculate the motion of the whole system. As the buoy is regarded as a rigid body, when Δt is very small, it is applicable to use Eq. 27and Eq. 28to estimate the movement of the buoy in every single time step. Attention is needed when considering the force components on the buoy. Like what is shown in Figure 39, the tension from the cables comes from the result calculated by MOORING3D in the previous time step.

$$u_t = u_{t-1} + \frac{F_{total}}{m} * \Delta t \tag{25}$$

$$\omega_t = \omega_{t-1} + \frac{Q_{total}}{I} * \Delta t \tag{26}$$

$$x_t = x_{t-1} + u_t * \Delta t \tag{27}$$

$$\theta_t = \theta_{t-1} + \omega_t * \Delta t \tag{28}$$

where u is the surge velocity for the center of gravity of the buoy. ω is the angular velocity in z direction. F_{total} and Q_{total} standfor the total force and moment exerted on the buoy's origin. m is the mass of buoy. I is moment of inertia for the buoy about the buoy's origin.

According to the model test result shown in Figure 40, in the surge free-decay model test, the initial position of the buoy's center of gravity starts at $x = -8\,m$ in the full scale, which is $x = -0.225\,m$ in the model scale. Under the influence from the cables and fluid, the buoy will oscillate in a natural period and the amplitude of the oscillation will decay as time goes by.

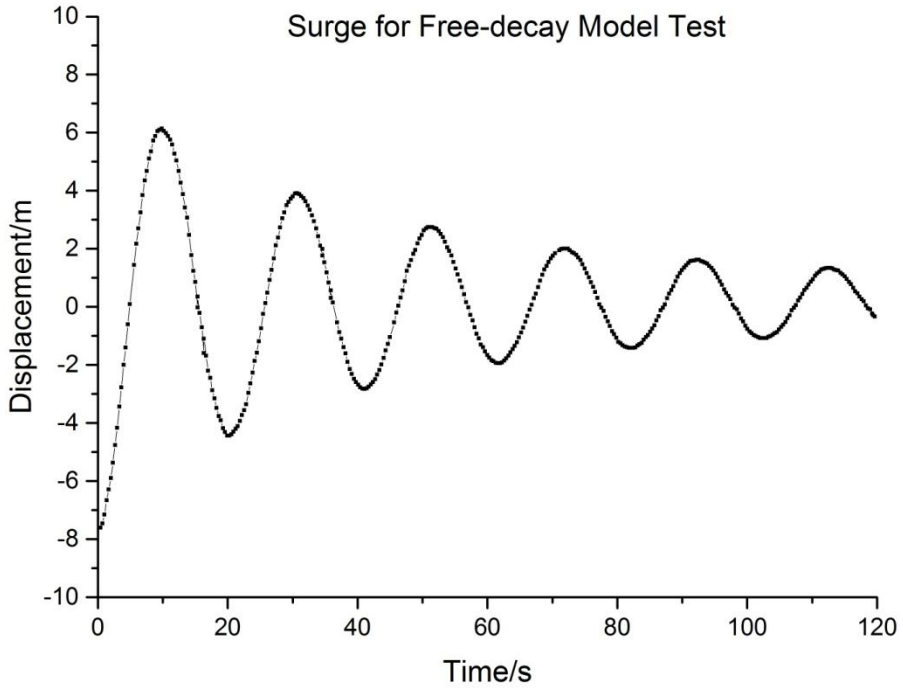

Figure 40. Surge Free-decay Model Test

Mooring Part

A lot of work has been done to adjust the parameters of the cable to matching the free-decay model test's result in Figure 40. Based on the design principle for the model test, the draft of the buoy must be kept as $5.65\ m$in full-scale size in static state, which provides a benchmark to modify the cable's parameters at the first step. Under the condition that the draft stays at $5.65\ m$, the initial displacement $x = -8\ m$ is set to the buoy. The surge displacement result calculated by the coupled code is compared with the test model's result in Figure 41. Since there was no big difference in the two results, another iteration of modification was not required.

The final comparison result is shown in Figure 41. Although these two sets of data cannot match to each other perfectly, the difference between these two curves is very small, which means that the model used in the coupled code has a similar hydrodynamic behavior to the model used in the model test. The final parameters for the mooring lines are listed in Table 4.

Table 4. Mooring Lines' Parameters in the Coupled Code

	Unit	New Mooring
Length	m	346.5
Wet Weight	te/m	0.375
Diameter	m	0.12
EA	metric tons	400.250
Normal Drag Coefficient		0.2
Axial Drag Coefficient		0.4
Normal Added Mass Coefficient		1
Axial Added Mass Coefficient		0.07

To provide a reference for further verification of the coupled code, another test with the same parameters for both buoy and cables is conducted with the commercial software Orcaflex. The results obtained from three methods are compared together and shown in Figure 41. To adjust the result from Orcaflex to the free-decay model test's result, the hydrodynamic coefficients of the buoy are set as the values shown in Table 5. It can be seen that by modifying the parameters in the code and Orcaflex, the surge displacements of the buoy's center of gravity are similar to each other.

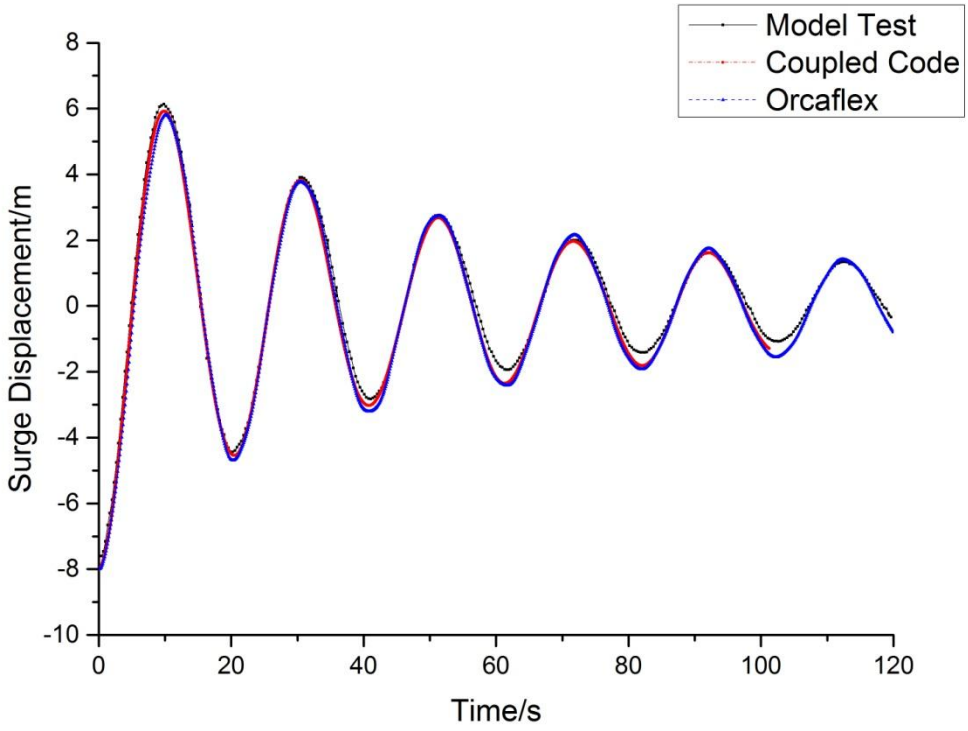

Figure 41. Surge Comparison in Free-decay Test

Table 5.Buoy's Coefficients in Orcaflex

	Unit	New Mooring
Normal Drag Coefficient		0.7
Axial Drag Coefficient		6
Normal Added Mass Coefficient		0.55
Axial Added Mass Coefficient		1

Simulation Result

The simulation time increment set in the free-decay test is 0.05s in prototype. As the model test only provides the results from 0s to 120s in the full-scale, the iteration steps is set to be 2400.

Figure 42 illustrates the comparison between Orcaflex and coupled code in the total force exerted on the buoy in surge direction. From the picture it can be seen that the curves of external forces on the buoy are similar with the period and amplitude of oscillation. But compared to the total force calculated in Orcaflex, the result from the coupled code is smoother, which means there exist more small oscillations in the total force calculated by Orcaflex.

We get similar conclusion when we compare these two methods in terms of hydro-forces on the buoy, which is shown in Figure 43. Compared to the results from Orcaflex which have lots of high-frequency ups and downs, the hydro-force obtained from coupled code is smoother, while these two forces are similar in the overall tendency, which keeps the surge motion of the buoy similar throughout the procedure.

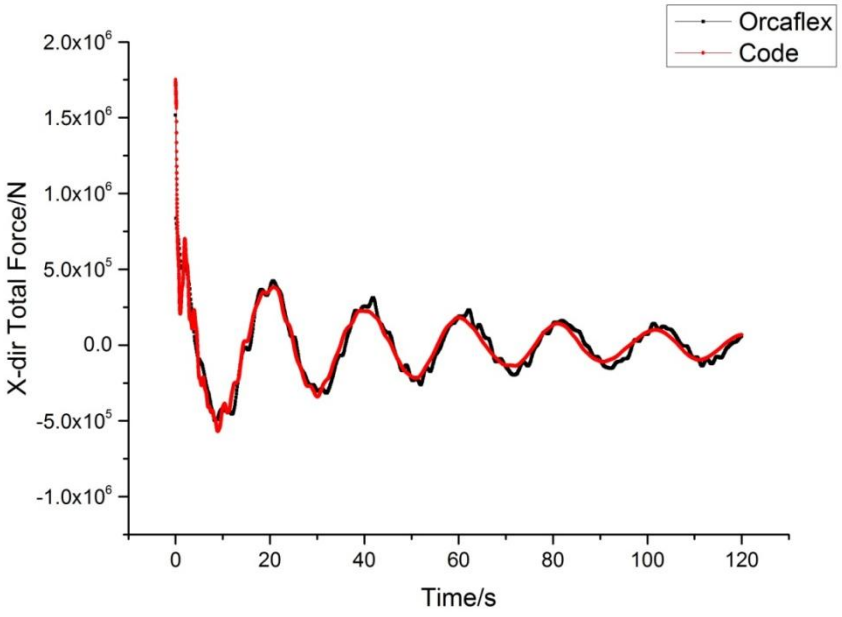

Figure 42. Total Force Comparison in x Direction

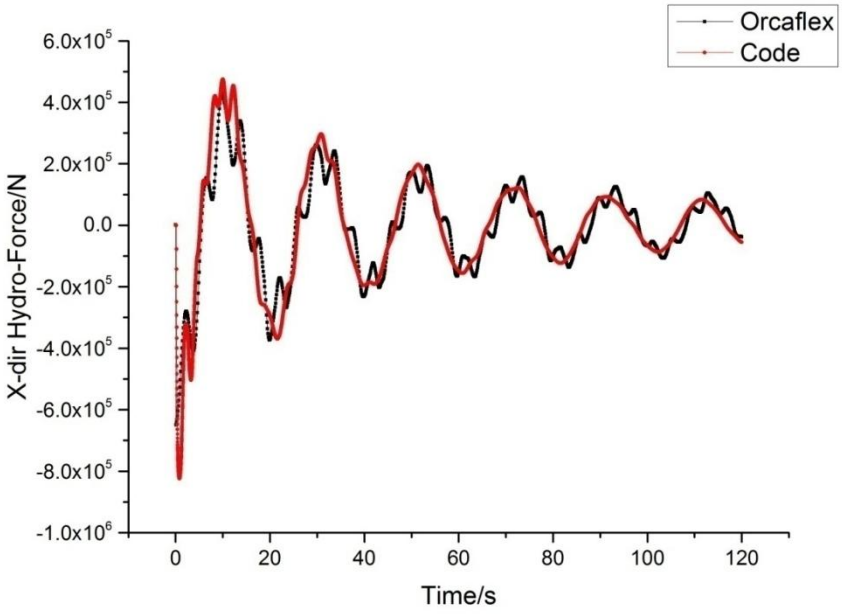

Figure 43. Hydro-Force Comparison in x Direction

One reason to explain the difference between the shapes of curves is that Orcaflex considers 6 degrees of freedom during the simulation while only the movement on the x-y plane is considered for this research, which means that heave, pitch and roll motions are neglected in the calculation. Although it has been specified that compared to the surge motion in the free-decay test, the vertical motions are comparatively small, the vertical displacement of the buoy still has effect on the hydro-force together with the cables' response. Figure 44 and Figure 45 show the heave motion and the heave-induced total force in z direction separately. From the pictures it can be seen that the heave motion oscillates mostly in the range of $[-0.02m, 0.02m]$ around the initial draft $-5.65\ m$ after the first 20 seconds, which is very small compared to the surge motion. Compared to the displacement in x direction, the ups and downs in vertical direction are not so regular, which results in the irregular pattern of vertical forces added on the buoy, including the oscillating changes in the cable tension. The irregular vertical force, although is not of the same order as the force in x direction, still has effect on the horizontal forces. Its irregular oscillations with short periods may be the reason why there exist many short-period oscillations in the curve of total force in and hydro-force in x direction. In conclusion, the high-frequency oscillations in the forces and displacement in z direction may not influence the forces and motions in x and y directions obviously, but it can have some small influence on the original motion on x-y plane.

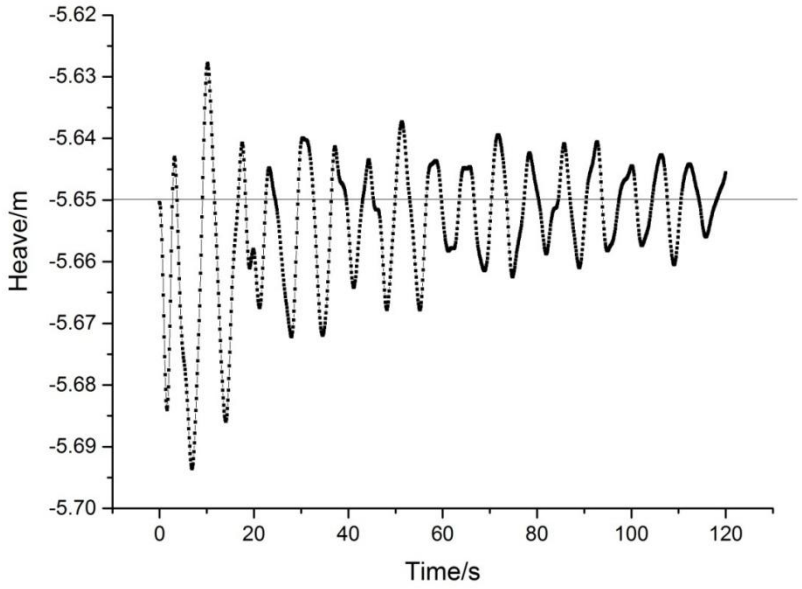

Figure 44. Heave Displacement in Orcaflex

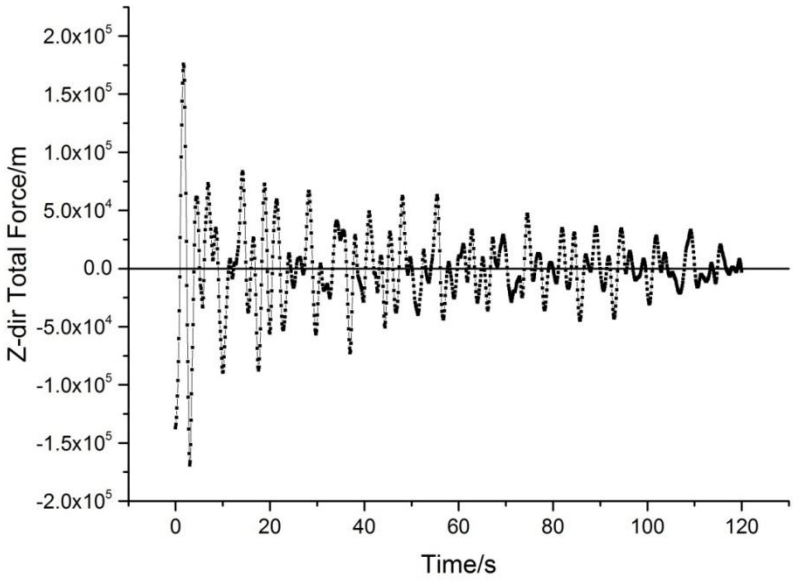

Figure 45. Total Force in z Direction in Orcaflex

Figures 46 to 50 illustrate the vorticity patterns in free-decay test with coupled code at simulation time step 100, 300, 500, 1300 and 2400, which correspond to full-scale time 5s, 15s, 25s, 65s and 120s. The contours with color show the location and direction of vorticity on the plane of z=-0.1, which is 1.7 meters below the free surface.

Compared with the surge displacement in Figure 46, when time is equal to 5 seconds, it is in the process of moving from leftmost position to positive x direction. As the buoy's position at this time is near to x=0m, the velocity of the buoy is near to the utmost positive value. It can be seen in Figure 46 that the vortex is mainly located on the downstream side of the buoy. And the contour of the vorticity is larger than the contours in previous steps. When it comes to 15 seconds, the buoy has already reached the farthest position in positive x direction and started to move backward. It can be seen that in Figure 47, new vortex has been generated on the other side of the buoy. As it takes some time for the previous vortex to decay, the vortex that developed in previous time steps still exists on buoy's upstream side. At t=25s, the buoy comes back to the rightmost position in the second period. An interesting phenomenon is discovered that in the fluid field away from the buoy, there appears some additional vortex gradually as time goes by. And with the time step increasing, the size of the vorticity pattern is becoming larger.

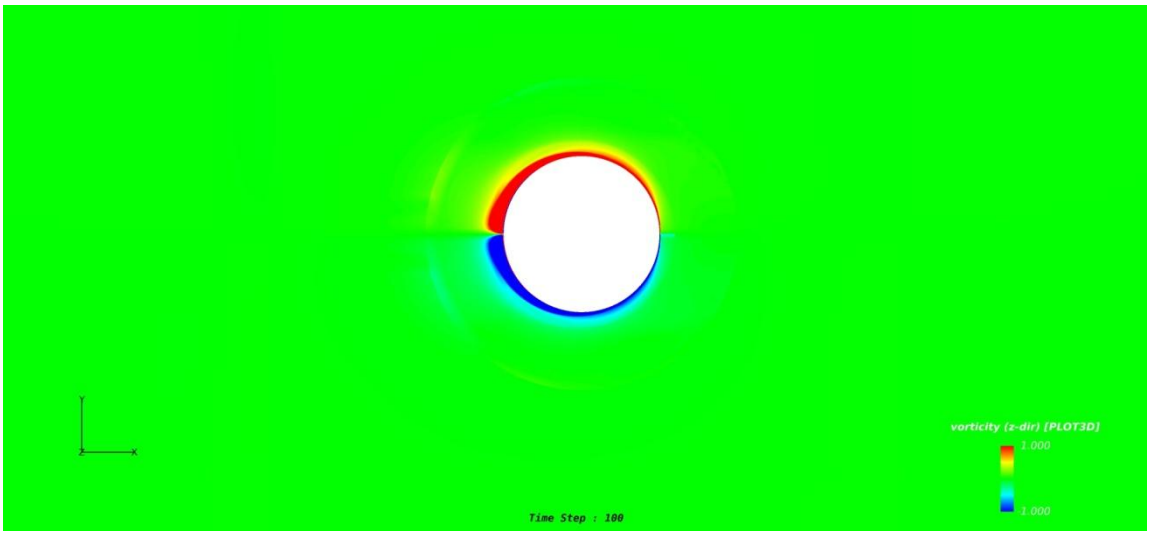

Figure 46. Vorticity Pattern in z Direction at T=5s

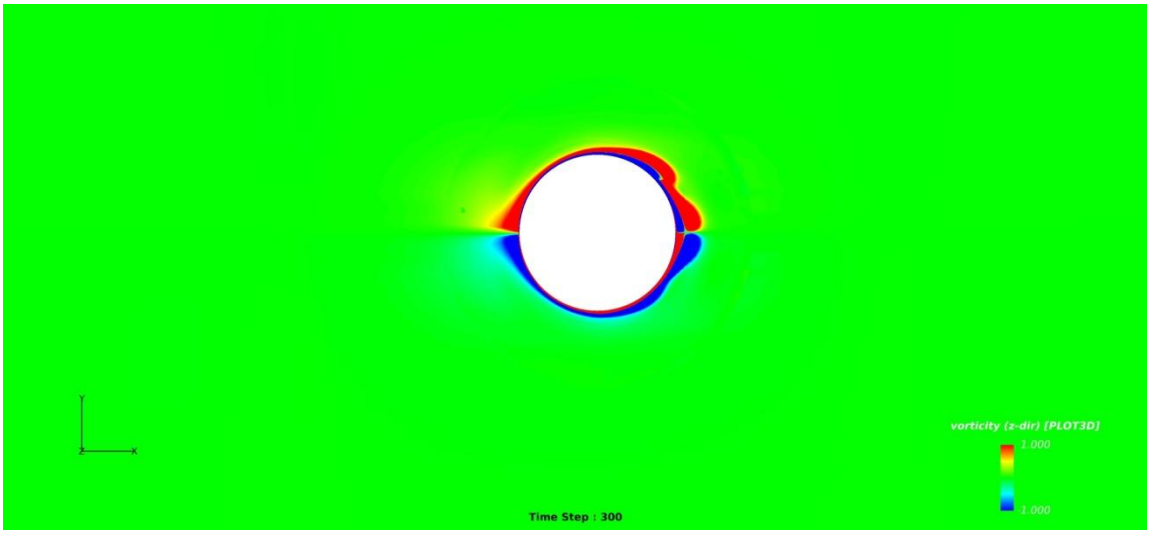

Figure 47. Vorticity Pattern in z Direction at T=15s

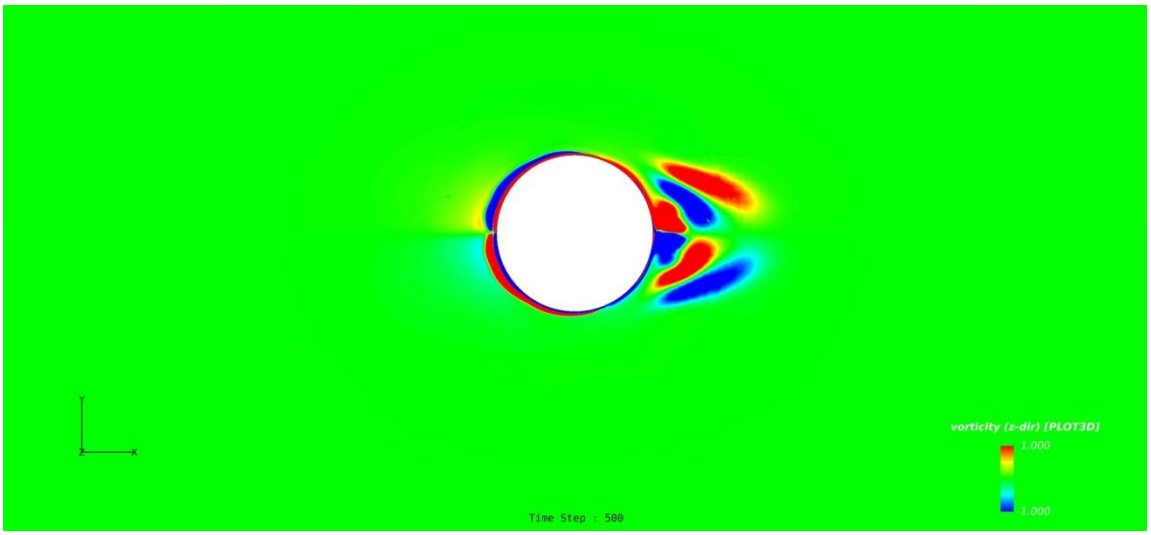

Figure 48. Vorticity Pattern in z Direction at T=25s

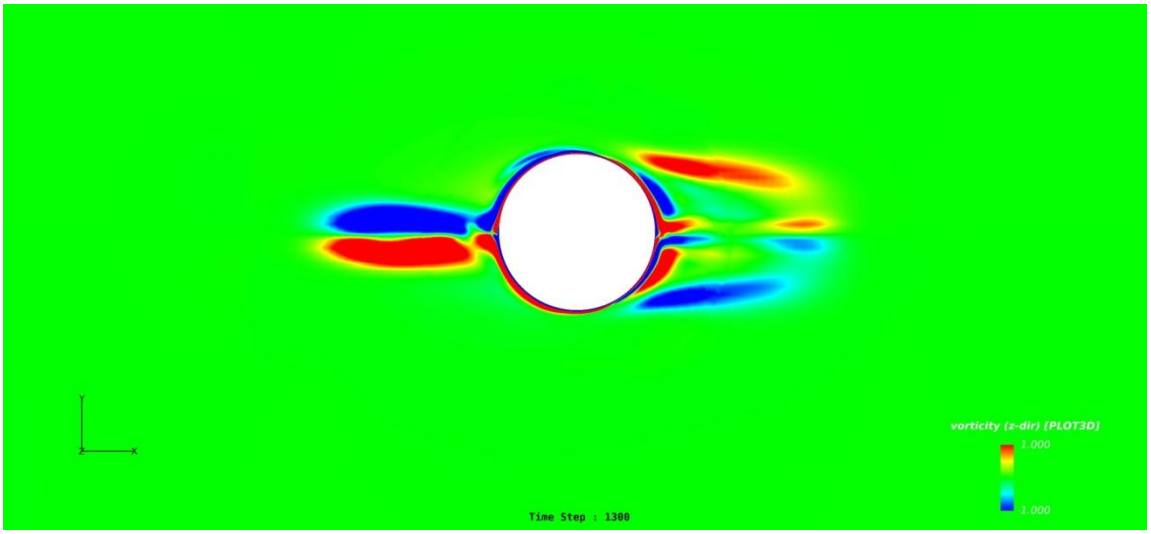

Figure 49. Vorticity Pattern in z Direction at T=65s

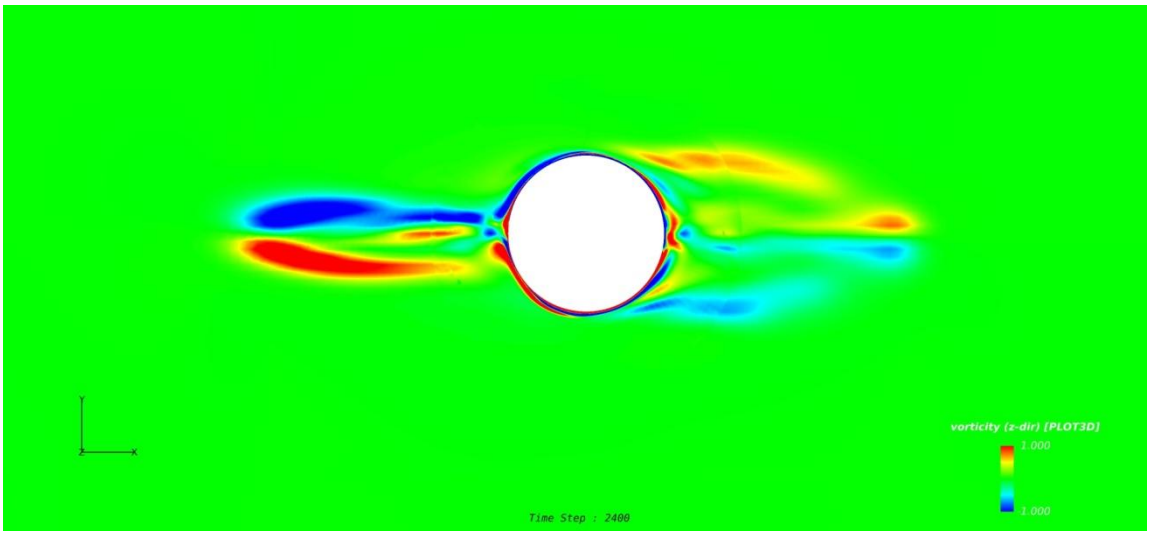

Figure 50. Vorticity Pattern in z Direction at T=120s

This phenomenon can be explained with a view of the vortex generation in z direction. Figure 51 illustrate the vortex contour on the fluid surface of z=-0.2. Comparing Figure 51 with the vortex pattern in Figure 48, it can be seen that the area of the vortex away from the buoy is larger and stronger on a deeper fluid surface. And the vortex is more complicated at z=-0.2 than z=-0.1.

Figure 52 presents how the fluid is moving on the vertical fluid plane. The cross section is selected at y=-0.2. The colored contours in the figure stand for the vorticity in y direction. The small arrows in the figure represent the direction of the fluid velocity at that point. As the buoy is reaching to the crest position of the second period in positive x direction, the fluid surrounding the buoy is still forced to move forward in positive x direction. Due to the limited height of the buoy's draft, some of the fluid is pushed down to the bottom of the buoy while some of the fluid is stimulated to go upward. The great change of the fluid's direction will produce vortex. That's why after certain time step,

there will appear some additional vortex in the position away from the buoy, which is pushed up from the fluid layer below by oscillating motion of the buoy. The vortex on the bottom of the buoy also has effect on the motion and hydro-force in z direction. It can be further studied if the vertical movement is taken into account.

This vorticity induced by upward fluid decays with time and the amplitude of surge motion. We can see from Figure 50, after 120 seconds, the surge motion of the buoy has become more trivial. The vortex existed before is almost disappeared.

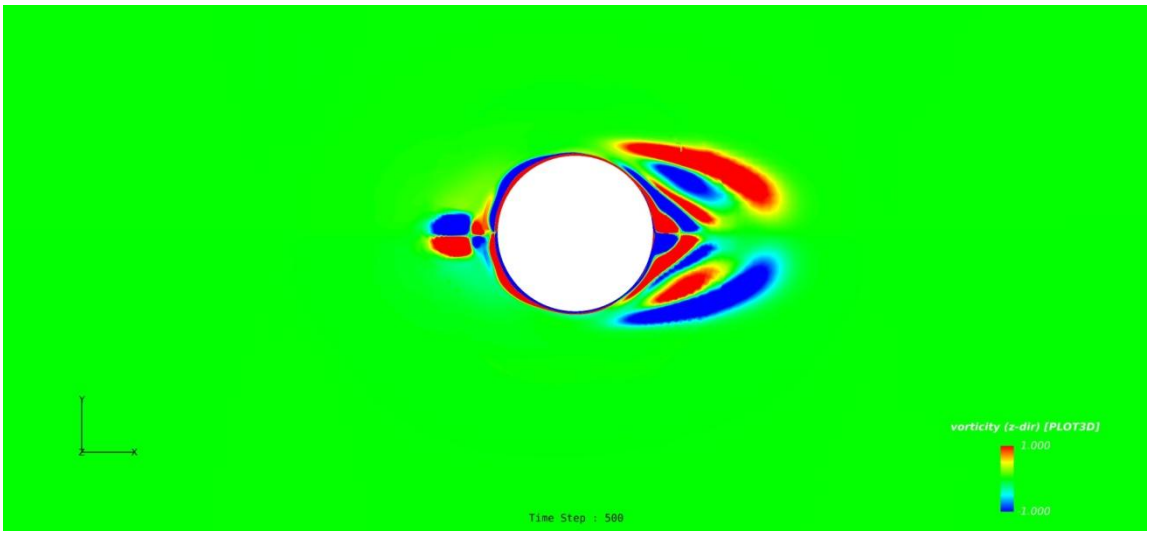

Figure 51.Vorticity Pattern in z Direction at T=25s (z=-0.2)

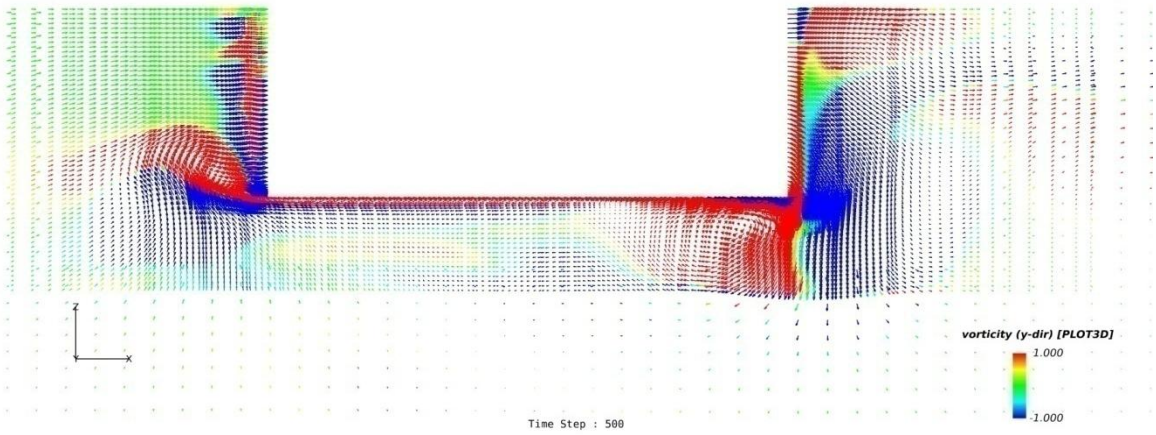

Figure 52.Vorticity Pattern in y Direction at T=25s (y=-0.2)

To sum up, in this chapter it has been shown that the coupled code is able to predict the hydrodynamic response of the CALM buoy system. By comparing its results with the results from model test and Orcaflex, we calibrate a CALM buoy system model with the similar behavior that can be used for further study. By analyzing the fluidic pattern generated by the code, we can see the coupled code is able to predict reasonable physical phenomenon in the free-decay test. The restriction of vertical movement has some effect on the prediction of horizontal dynamic responses, while the overall behavior of the buoy is similarly to the one in Orcaflex, which indicates that the coupled code and the buoy model can be used to study under other conditions.

Parameter Study

As for the input of the simulation, parameters like grid refinement and time increment for simulation should not be the factor to influence the final result calculated by the coupled code method. To make sure that the results are independent of these two parameters, controlled trials are conducted to verify in two aspects which are the grid refinement and time increment separately.

Grid Refinement Study

A grid refinement study is conducted with different resolutions of grids in the fluid domain surrounding the buoy model. The resolution is mainly controlled by two parameters Δθ and Δr, whose meanings are illustrated in Figure 53.

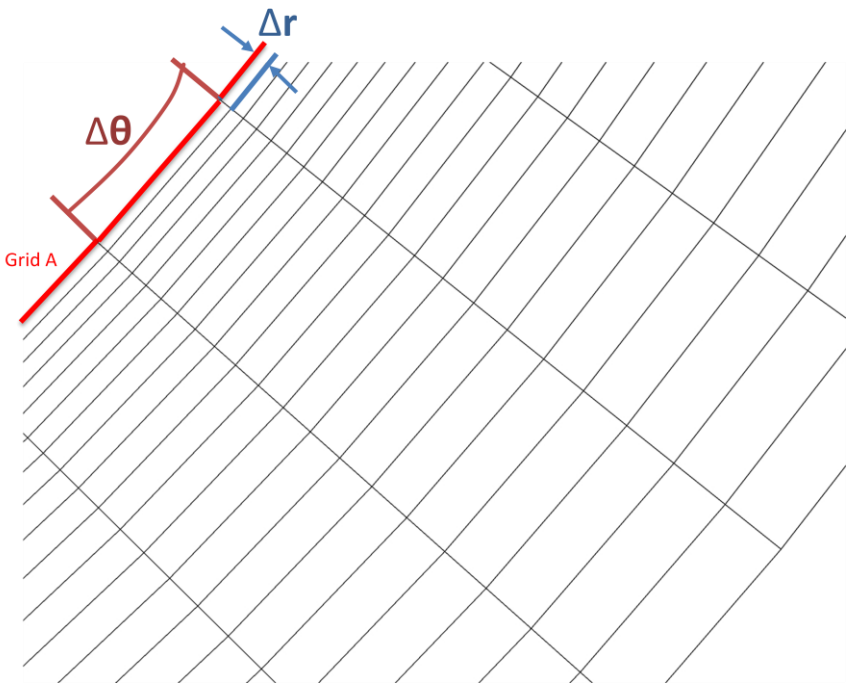

Figure 53. Zoomed View of the Grid surrounding the Boundary of the Buoy

Figure 53 is a zoomed view of the grid surrounding the circumferential boundary of the buoy. The red grid line named Grid A stands for the boundary of the buoy. $\Delta\theta$ is the included angle between two adjacent grid lines in centripetal direction. Δr is the distance between the 1st grid line (the boundary of the buoy) and the 2nd grid line in the circumferential direction. By adjusting the values of $\Delta\theta$ and Δr, the resolution of the grid is changed. For the grid refinement study, two more cases with $\Delta\theta = 2.25°$, $\Delta r = 0.001D$ (fine grid case) and $\Delta\theta = 4.5°$, $\Delta r = 0.002D$ (coarse grid case) are conducted to compare with the case with medium grid resolution used throughout the research with $\Delta\theta = 3.0°$ and $\Delta r = 0.002D$ (Table 6). D is the diameter of the buoy model.

Table 6. Values of $\Delta\theta$ and Δr for Different Grid Resolution

	$\Delta\theta$/Intervels	$\Delta r/D$
Fine Grid	$2.25°/160$	0.001
Medium Grid	$3.0°/120$	0.002
Coarse Grid	$4.5°/80$	0.002

With the change of $\Delta\theta$ and Δr, the total number of the grids is also changed. The numbers of grids for the three cases are shown in Table 7.

Table 7. Numbers of Grid for Different Grid Resolution

	Near Body	Off Body
Fine Grid	722385	1424130
Medium Grid	521633	1223378
Coarse Grid	359113	1060858

The comparison between the three cases in terms of surge displacement is shown in Figure 54. From the figure it can be seen that the change of grid resolution doesn't have much effect on the final result, which means that estimation provided by the coupled code is independent of the grid resolution and the grid with medium resolution is applicable for other study.

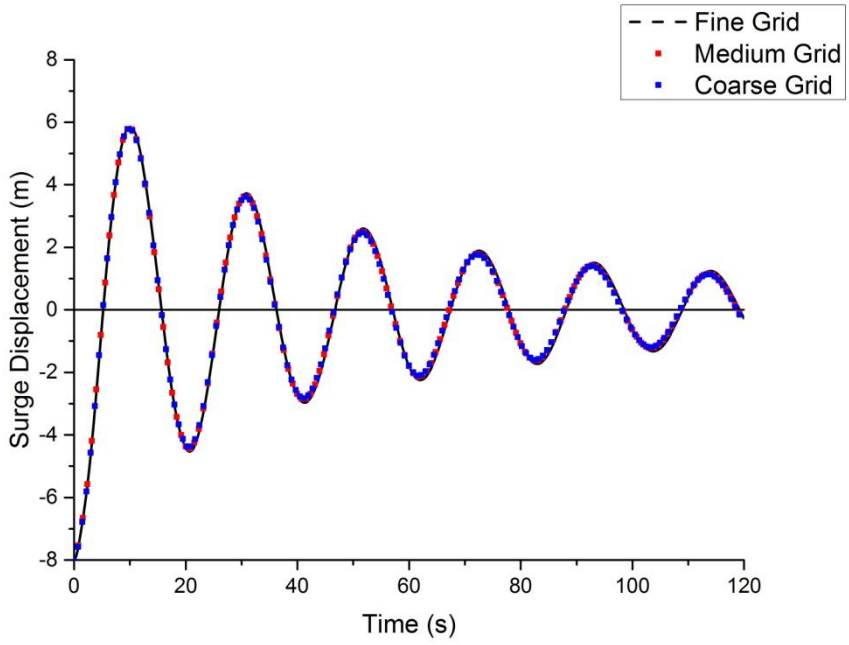

Figure 54. Comparison of Surge Displacement with Different Grid Resolution

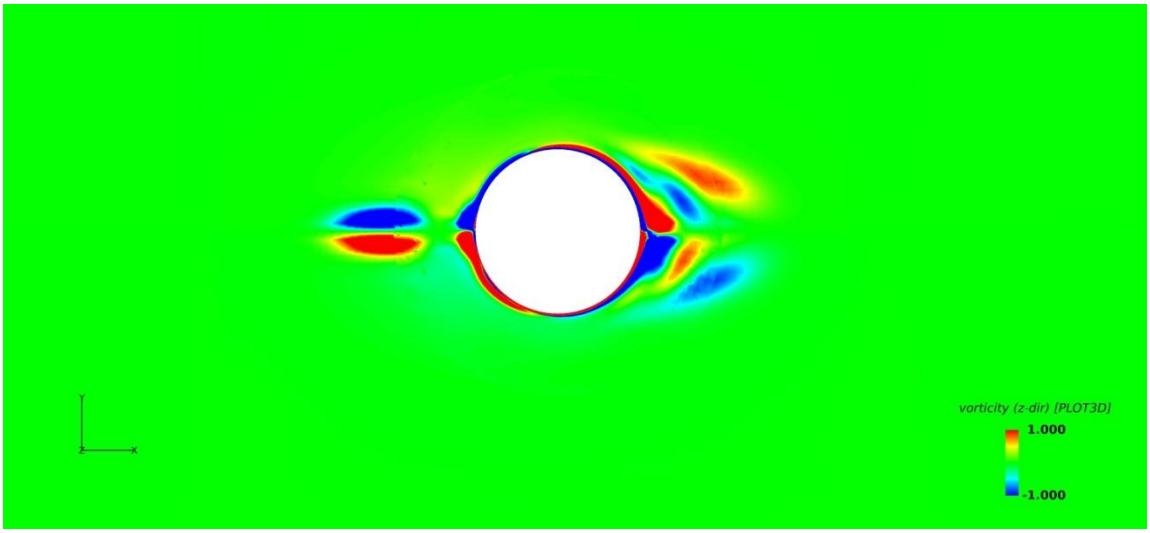

Figure 55. Vorticity Pattern at Time=35s with Coarse Grid

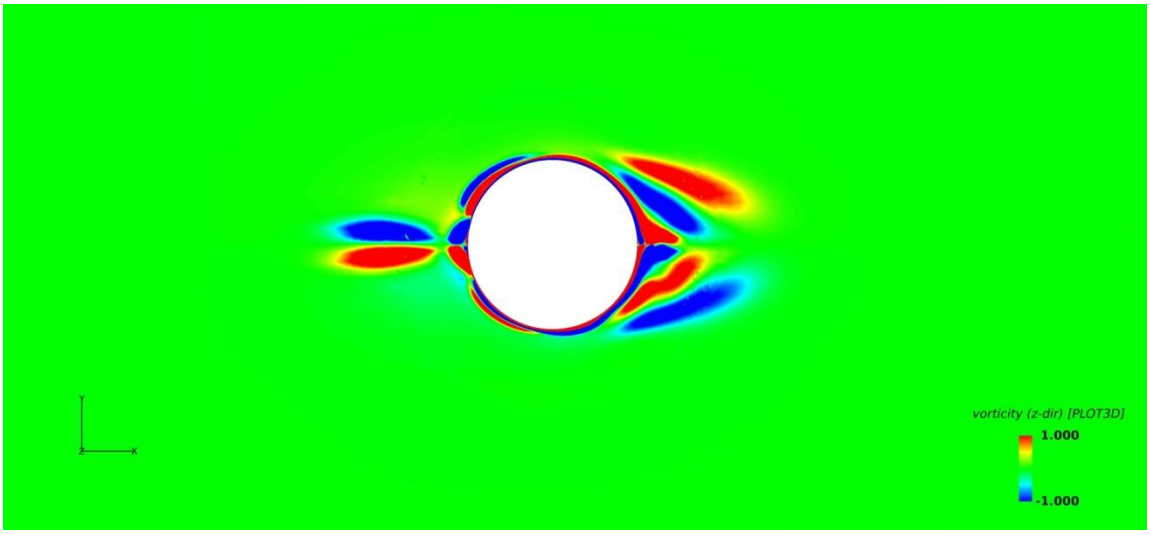

Figure 56. Vorticity Pattern at Time=35s with Medium Grid

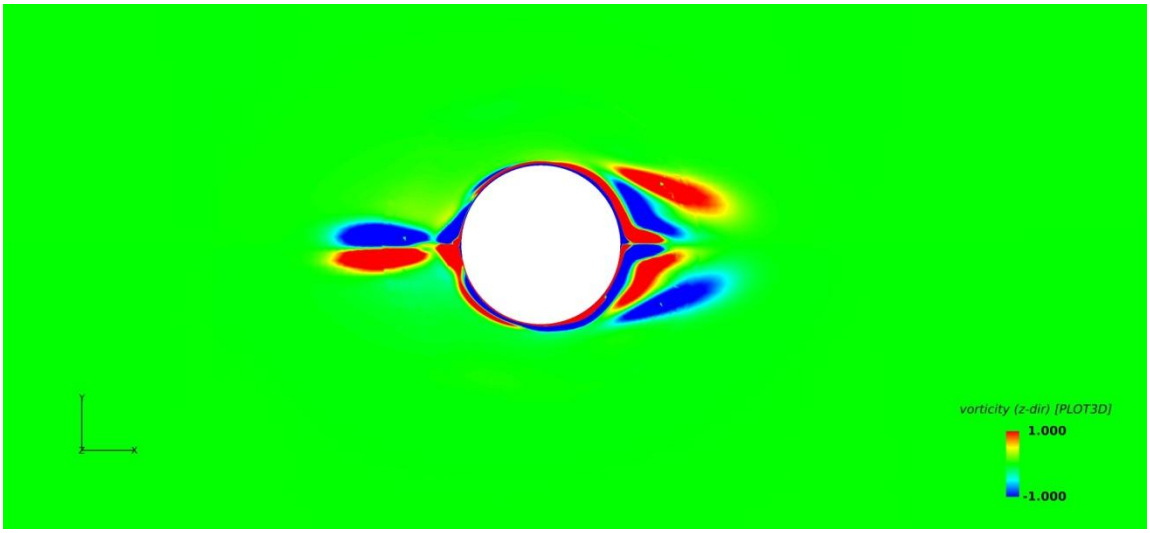

Figure 57. Vorticity Pattern at Time=35s with Fine Grid

Figures 55, 56 and 57 illustrate the vorticity patterns generated with different grid resolutions at full-scale time equal to 35s. By comparing the three figures it can be seen that there exist some small differences in the vortex contour, while the constitution of the contour looks very similar, which indicates that the grid resolution has only a little bit effect on the simulation of vorticity.

Time Increment Study

Another study is conducted to confirm that the results are independent of time increment at each time step for simulation. The time increment previously used for free-decay test is 0.05s. A controlled trial with time increment equal to 0.01s is conducted simultaneously for comparison. The comparison between the two cases in terms of surge displacement is shown in Figure 58.

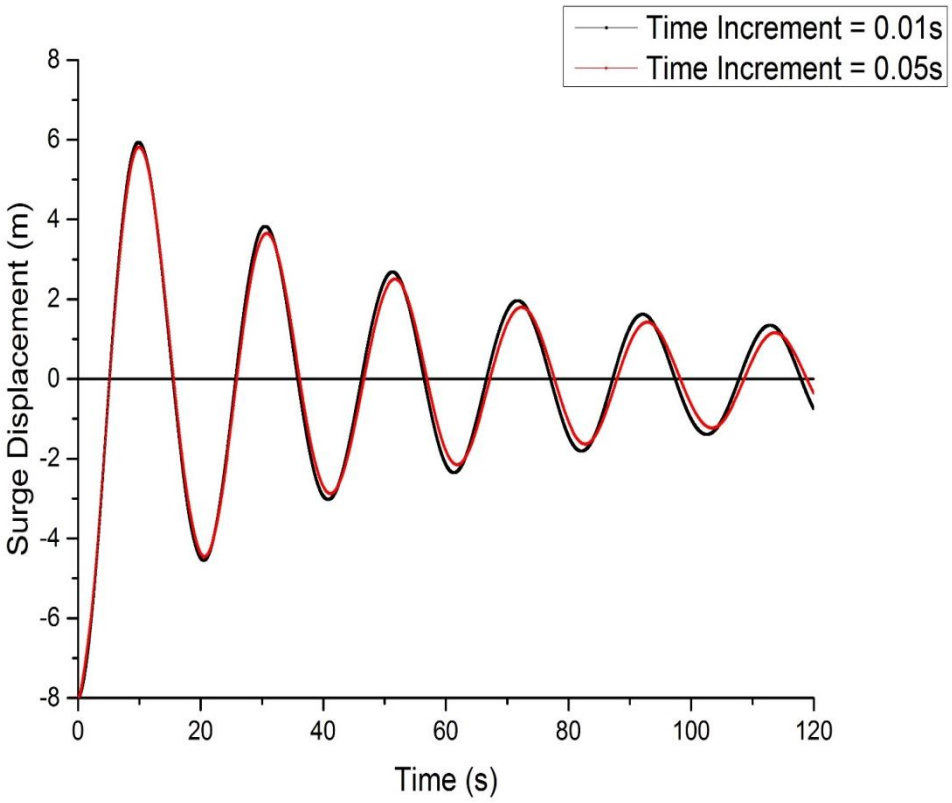

Figure 58. Comparison of Surge Displacement with Different Time Increment

From the picture it can be seen that the change of time increment doesn't have much effect on the final results simulated by the coupled code method, which means that the simulation with time increment equal to 0.05s is accurate enough.

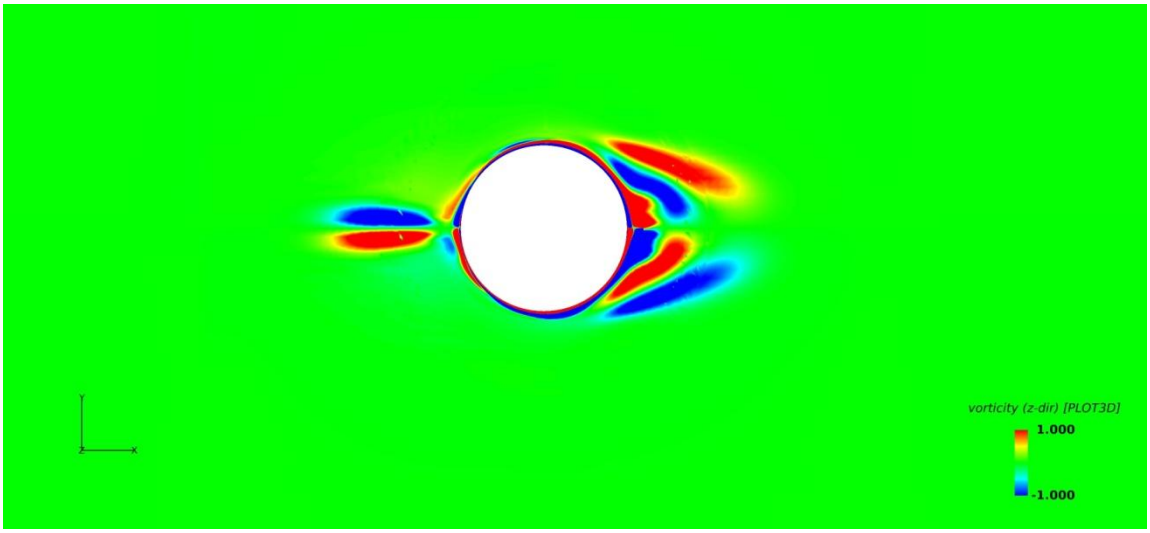

Figure 59. Vorticity Pattern at Time=35s with Time Increment=0.01s

Figure 59 illustrate the vorticity contour around the buoy at full-scale time equal to 35s with a smaller time increment of 0.01s. By comparing this figure with Figure 56, it can be seen that there exist some slight difference between the two cases with different time increments. Considering the displacement of the buoy is not exactly the same at the same time shown in Figure 58, it's reasonable that there exist some difference between the two patterns. As the difference is very small, it can be inferred that the time increment doesn't have much influence on the simulation of vorticity.

According to the results obtained from Grid Refinement Study and Time Increment Study, it can be concluded that the results we get from the free-decay test simulation are reasonable and accurate under the condition of medium grid resolution and time increment equal to 0.05s. The coupled code method and the model are calibrated correctly for the following study.

CHAPTER IV

SIMULATION UNDER UNIFORM CURRENT CONDITION

With the work that has been done in Chapter III, a CALM buoy system has been modeled with similar dynamic response to the CALM buoy system in model test and Orcaflex. The focus of this chapter is on studying the prediction of the hydrodynamic responses of the buoy under a constant uniform current condition. The model used in this chapter is the same as the one in Chapter III. By analyzing the simulation result, it can be verified that the coupled code is able to predict reasonable behaviors of the buoy under uniform current circumstances.

Experiment Set-up

At the initial time step, the buoy stays static at the origin of the global coordinate. Then it starts to face a uniform current from the far field in x direction (Figure 60). Under the influence of the mooring system, the buoy is forced to have periodic oscillation in x direction and it is foreseeable that the amplitude of the oscillation will decay until the external force on the buoy is balanced. A comparison is made between the coupled code and Orcaflex in terms of the simulation of the buoy's hydrodynamic responses. By analyzing the result, the ability of the coupled code method to simulate the dynamic behaviors of the buoy under uniform current conditions is verified.

Buoy Part

As the aim in this chapter is to verify that the code is able to predict the same CALM buoy system under uniform current condition, the CALM buoy system model is the same as the one used in Chapter III. Unlike setting an initial displacement in the free-decay test, the external force on the buoy is balanced. The buoy is kept static at the origin of the global coordinate on x-y plane. The draft of the buoy is kept at 5.65 m in the full-scale size. Like what is shown in Figure 60, from the far field there comes a steady current whose velocity in z direction is also uniform.

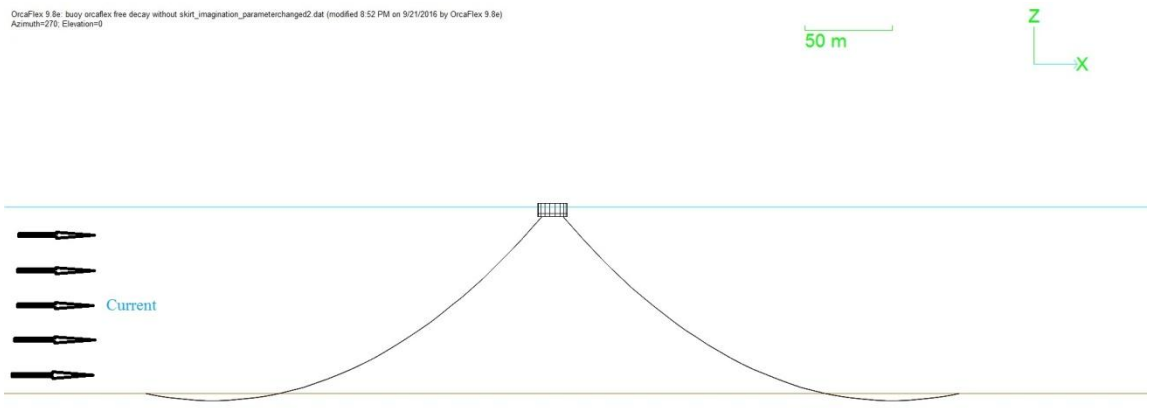

Figure 60. Side View of the Test Under Current Condition

The motion of the buoy is simulated by the motion module which is the same as the one used in the free-decay test. All the grids are regarded as one uniform block. The block is set to move together with the buoy model.

Mooring Part

Similar to the buoy part, the mooring system keeps the same parameters as the one used in free-decay test. One difference is that the fairlead positions of the mooring lines are synchronized with the motion of the buoy, so that at first step the total tension in horizontal direction from the four mooring lines should be 0. The buoy is kept static before the current comes.

Another difference is that the influence of the current is not only exerted on the buoy, but also on the mooring systems. The current will have continuous effect on the slender rods, which correspondingly influences the cable tension on the buoy. As a result, the dynamic responses of the whole system are affected.

Simulation Result

To verify the accuracy of prediction with the coupled code method, the same test is also conducted with Orcaflex. Both of the simulations are based on the same input and parameters. The final results are compared and analyzed below.

The calculation time step is set to be 21800, with a dimensionless time increment of 2.94e-3, which is 0.05 s in prototype. The complete full-scale simulation time is around 1100 s. The full-scale current velocity in this simulation is 1 m/, which is equivalent to dimensionless current velocity 1 in the FANS code. The current velocity is also 1 m/s in the MOORING3D code. The comparison between the coupled code and Orcaflex in terms of surge displacement is shown in Figure 61 and Figure 62.

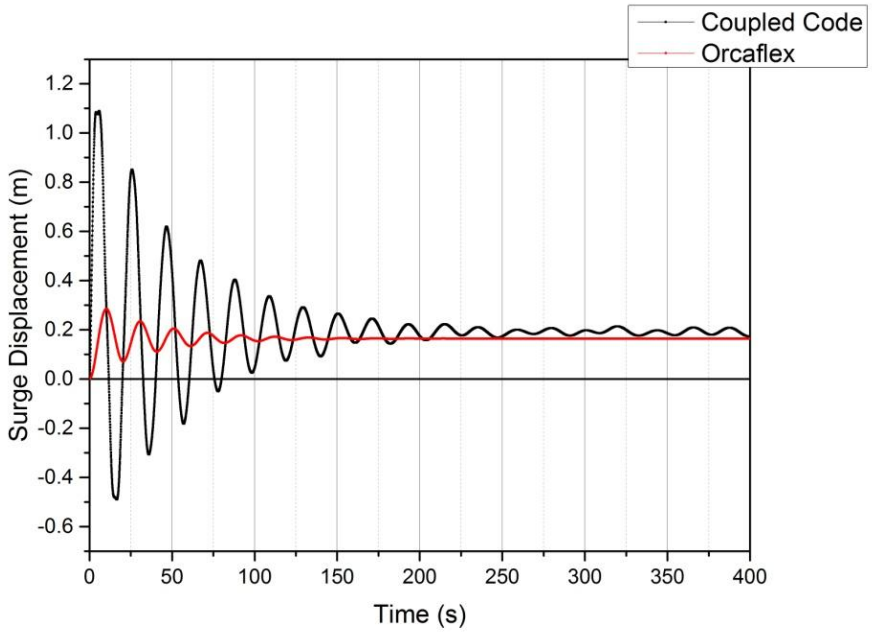

Figure 61. Surge Comparison under Current Condition

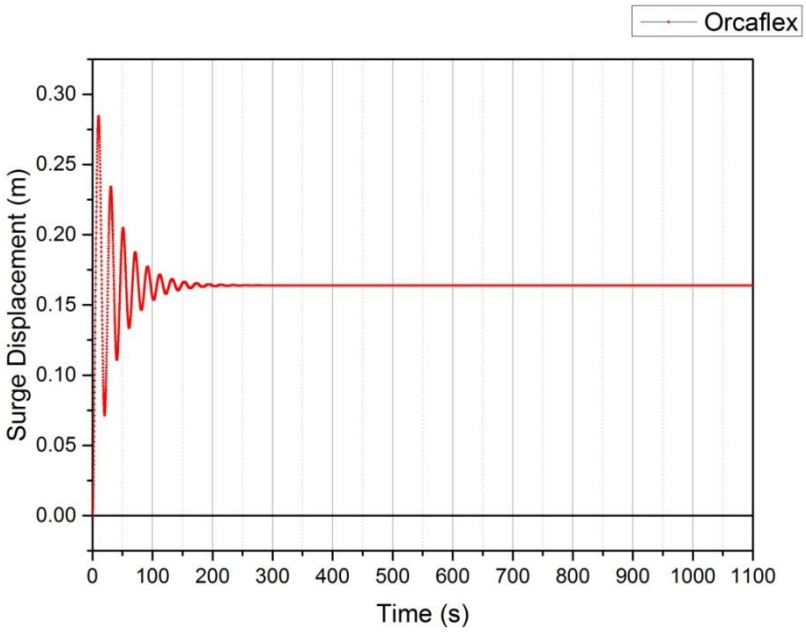

Figure 62. Surge Displacement in Orcaflex

Figure 63 shows the comparison between Orcaflex and the coupled code method in terms of surge displacement during the time from 0 s to 400 s. From this picture it can be seen that the period of oscillation in the coupled code is still similar to the one in Orcaflex. However, great differences exist in the surge displacements between the method of coupled code and Orcaflex. Compared to the amplitude of oscillation simulated in Orcaflex, the amplitude in the coupled code is much larger. After time is over 200 seconds, the surge motion in the Orcaflex turns into a constant value after several periods of decay (Figure 62), while the surge displacement oscillates with the amplitude in a relatively stable range. In the coupled code, the mean position around which the buoy oscillates is also a little bit higher than the stationary position in Orcaflex.

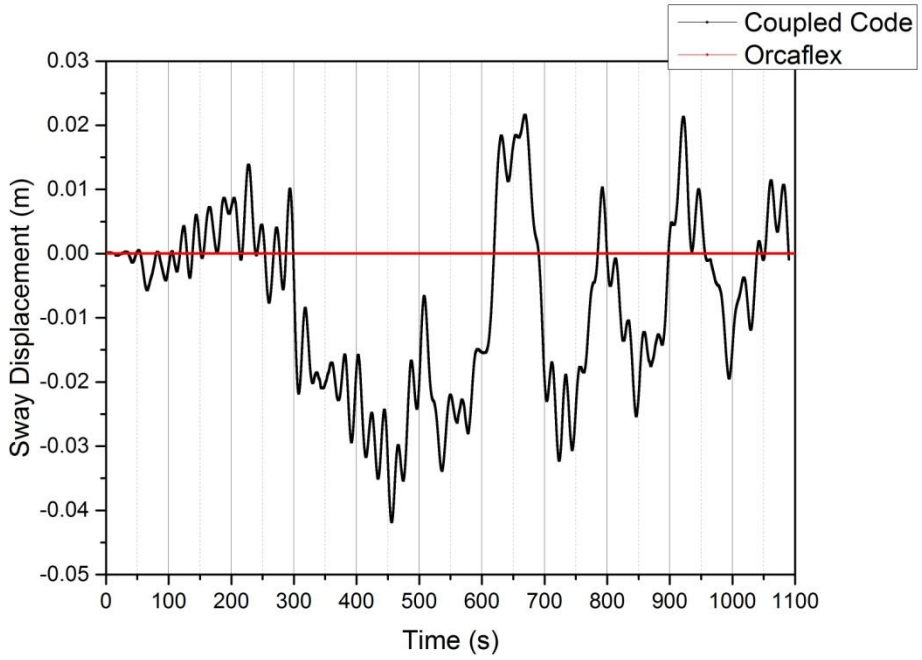

Figure 63.Sway Comparison under Current Condition

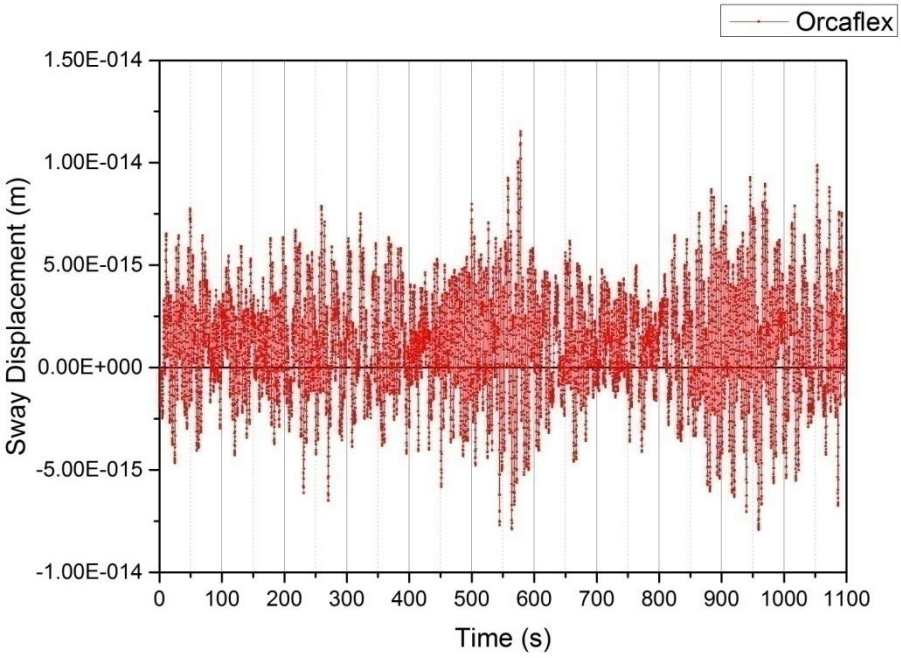

Figure 64. Sway Displacement in Orcaflex

In the aspect of sway motion, from Figure 63 it can be seen that compared to the amplitude of the sway motion in the coupled code, the sway displacement simulated in Orcaflex is too small to observe. Figure 64 shows that the range of the sway displacement lies between 1e-14 m and -1e-14 m, which can be regarded as 0 m. Although the amplitude of sway motion in the coupled code is much larger in comparison with the one in Orcaflex, considering the range of oscillation in surge movement and the size of the buoy, the sway motion is trivial.

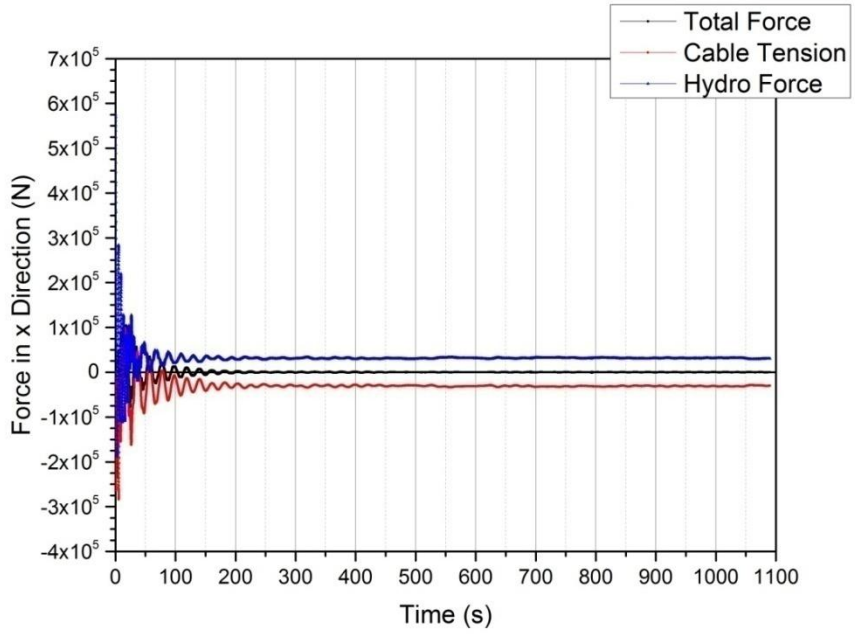

Figure 65. Forces in x Direction (Coupled Code)

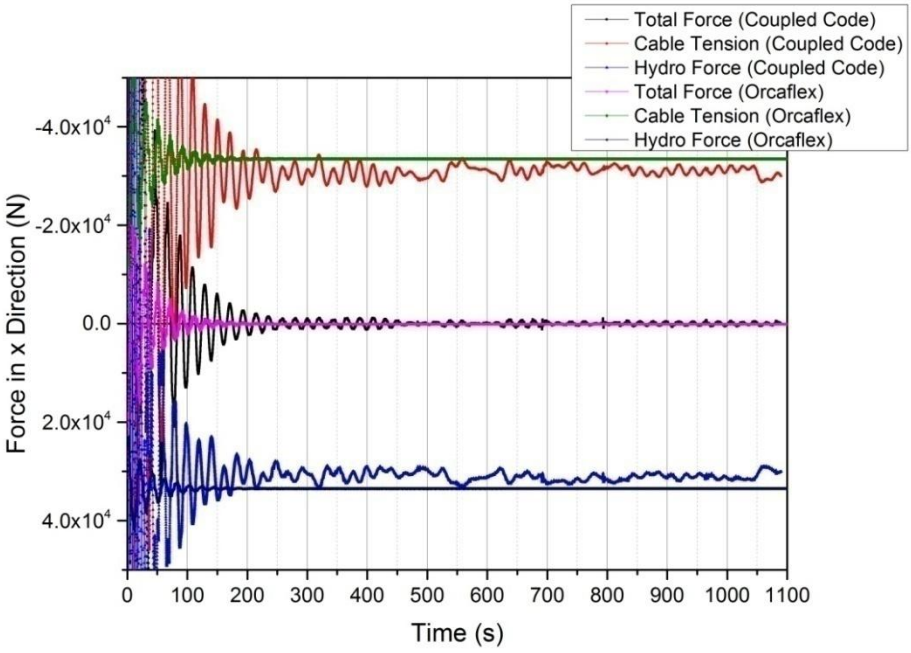

Figure 66. Forces in x Direction (Orcaflex)

Figure 65 illustrates the total force and its components' relation on the buoy in x direction simulated by the coupled code. Figure 66 depicts the physical quantities predicted by Orcaflex. From these two pictures it can be seen that once the buoy turns into a stable state after 200 seconds, the hydro/cable force in the coupled code is almost the same as that in Orcaflex. The mainly difference exists in the first 200 seconds. The hydro force and cable tension simulated by the coupled code is much larger than that simulated in Orcaflex, which matches to the difference between the coupled code and Orcaflex in terms of the behavior of surge displacement in Figure 61. As the buoy keeps oscillating in the simulation from the coupled code, the forces exerted on the buoy in x direction also move back and forth correspondingly.

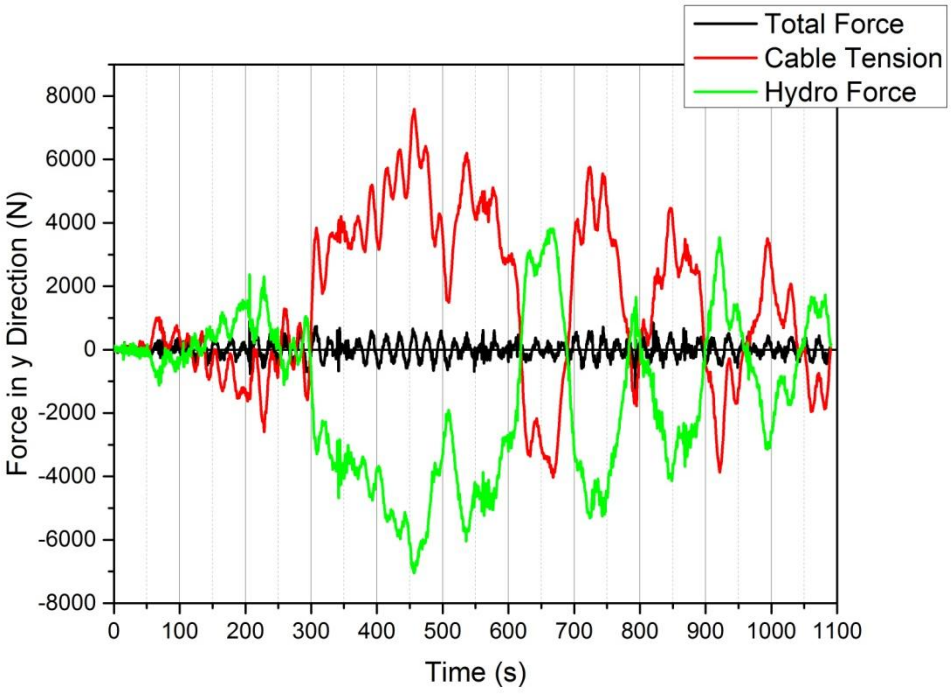

Figure 67. Forces in y Direction (Coupled Code)

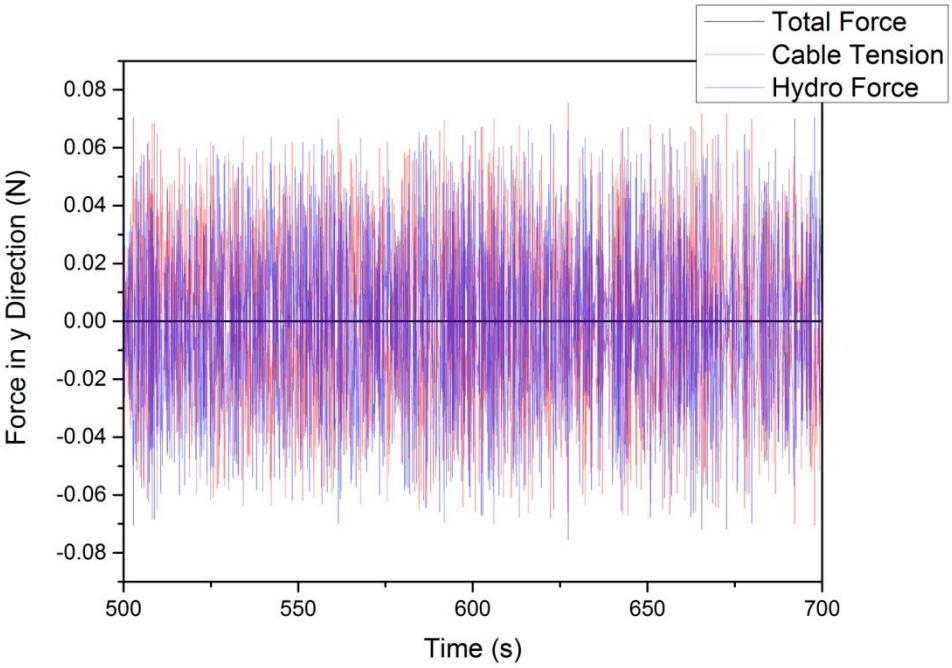

Figure 68. Forces in y Direction (Orcaflex)

Figure 67 shows the forces applied on the buoy in y direction in the coupled code. It is compared with scatter pattern Figure 68 which depicts the same variables in Orcaflex. Compared to the cable tension and hydro force exhibited in Figure 67, the cable tension and hydro force simulated in Orcaflex (Figure 68) are in such a small range that can be regarded as 0. Combined with the displacement pattern in Figure 64, it can be inferred that there is no motion or hydrodynamic forces in y direction in the simulation from Orcaflex.

Figures 69 to 72 show the vorticity pattern on the surface of z=-1.7 m at full-scale time 101s, 300s, 655s and 970s, which stand for four stage of the whole procedure.

By comparing the vortex pattern with the sway displacement in Figure 63, it can be inferred that the vorticity plays an important role in the movement of the buoy in y direction. At time equals to 101 s, the vortex is newly generated. The vortex patterns on the crossflow sides of the buoy are in an opposite direction, and their contours is similar to each other, which means that the vorticity at this stage is almost symmetric along the streamline of y=0. Due to the symmetry of the vortex, the displacement of the buoy in y direction is very trivial along the axis y=0.

After the vortex develops for some time, it comes into an unstable stage where exists many chaos in the flow. The vortex is no longer symmetric and changes irregularly. Any small disturbance may result in a different fluidic situation. That is the reason why the sway displacement changes drastically at this time.

Figure 71 shows that at 655 s, vortex shedding is generated on the streamwise side of the buoy. The vortex begins to dominate over each other alternatively, which brings about a periodic oscillation of the motion in y direction. As is shown in Figure 63, the sway displacement becomes relatively periodic around the x=0 axis, and the period is around 100 seconds, which is close to the period calculated by Strouhal number.

With the analysis above, it can be seen that the vortex is quite influential in the motion of the buoy, especially in the crossflow direction. In the aspect of surge motion, with vortex added on the streamwise side of the buoy, the motion in x direction is also influenced. That’s why the results of the displacement simulated in the coupled code and Orcaflex are different, as vortex is not considered in the simulation by Orcaflex.

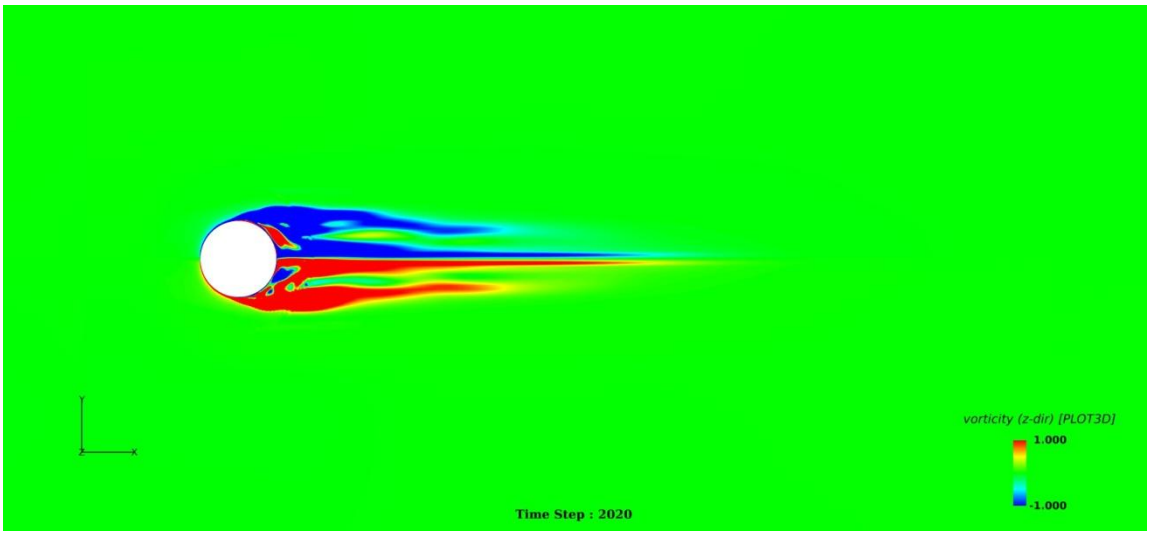

Figure 69. Vorticity Pattern at T=101s

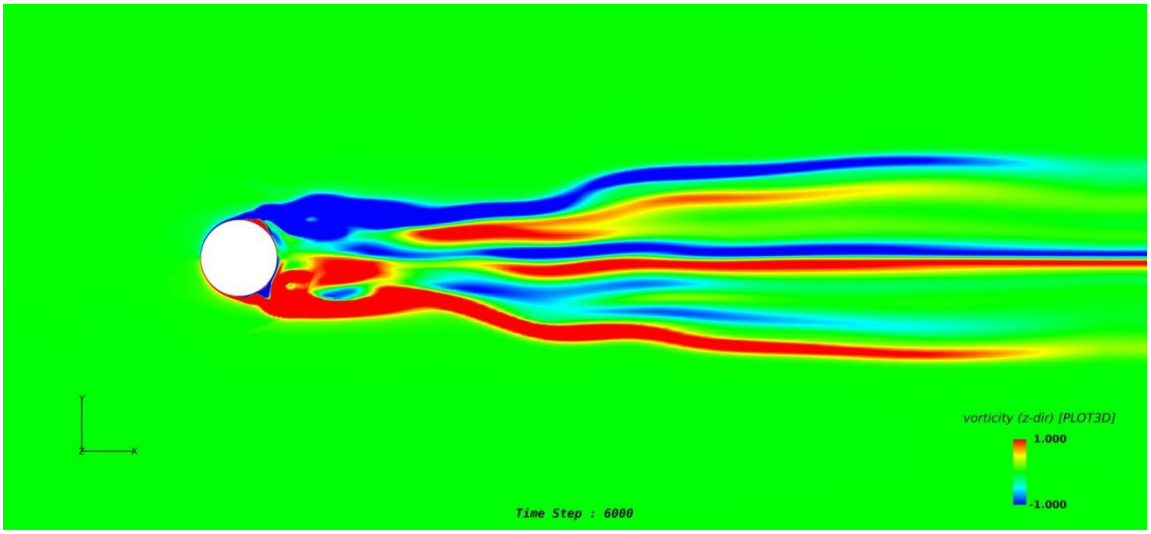

Figure 70. Vorticity Pattern at T=300s

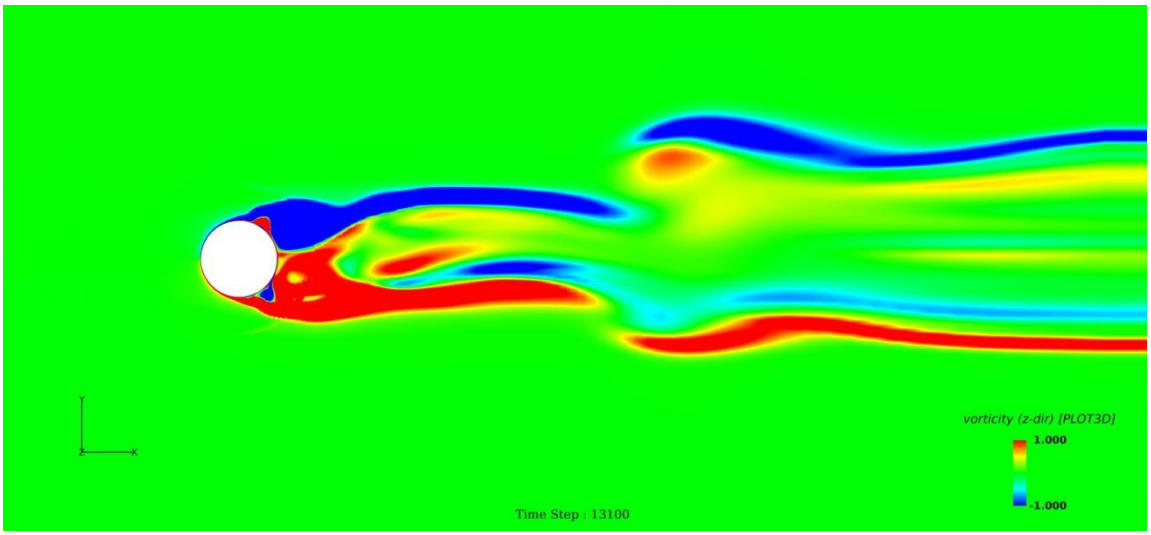

Figure 71. Vorticity Pattern at T=655s

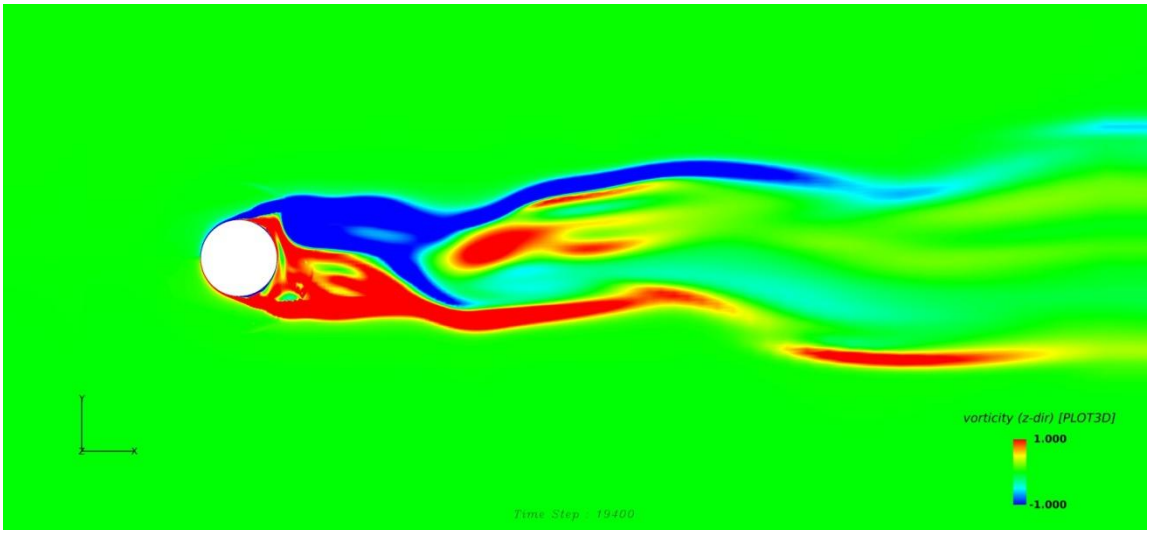

Figure 72. Vorticity Pattern at T=970s

CHAPTER V

SIMULATION UNDER DIFFERENT CURRENTS CONDITIONS

It has been verified that the coupled code is able to provide an accurate estimation of the hydrodynamic behaviors of the CALM buoy system under the condition of the uniform current according to the results from Chapter III and Chapter IV. The focus of this Chapter is on simulating the vortex-induced motion responses of the CALM buoy system by conducting several cases under the conditions of different current velocities.

Experiment Set-up

The CALM buoy system model is the same as the one used in Chapter IV. At the initial time step, the buoy stays static at the origin of the global coordinate. The direction of the incoming uniform current is same as the one in Chapter IV(Figure 60). To study the correlation between the amplitude of vortex-induced motion of the buoy and the current velocity, current velocities of 0.5m/s, 1m/s, 2m/s and 3m/s are used as different experimental conditions in different cases.

Simulation Result

According to different current velocities, the time increments for simulation are also different. Table 8 shows the corresponding time increment for each current velocity.

Table 8. Current Velocities and Corresponding Time Increment

Current Velocity (m/s)	Time Increment (s)
0.5	0.08
1	0.05
2	0.05
3	0.02

The range of time within which the results of the 4 cases are compared is from 0s to 1200s in prototype. Figure 73 shows the comparison of the displacements in x direction under the condition of different current velocities. Figure 74 shows the comparison of the displacements in y direction under the condition of different current velocities.

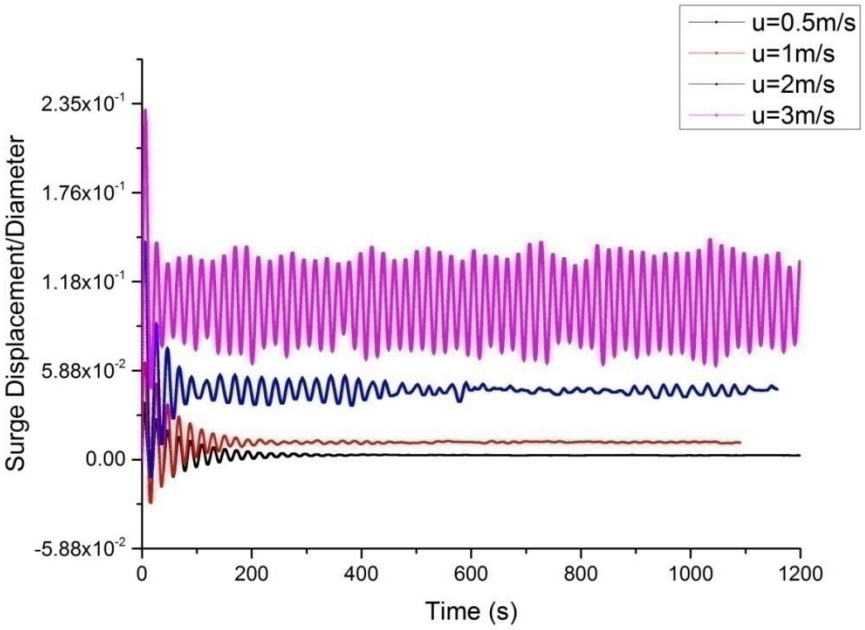

Figure 73. Comparison of Surge Displacement under Different Current Velocities

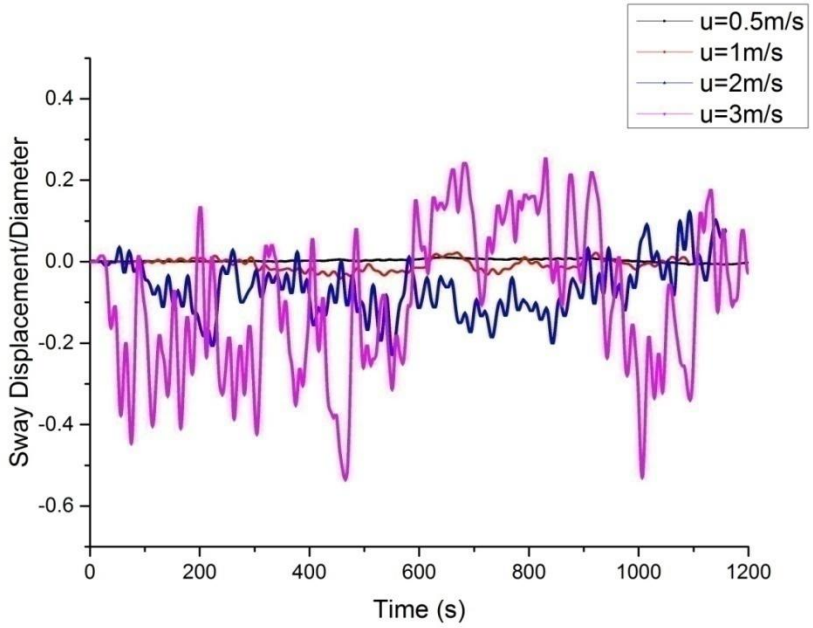

Figure 74. Comparison of Sway Displacement under Different Current Velocities

From Figure 73 and Figure 74, it can be seen that there exist some correlations between the displacements of the buoy and the current velocities. With the increment of the current velocity, the amplitudes of the oscillations of the buoy's displacements in both x and y directions increase as well. Due to the drag influence of the current, the mean positions around which the buoy oscillates in x direction also increases with the growth of current velocities. Different from the displacements in x direction, the displacements in y direction are mainly caused by the generation of vortex and vortex shedding, which can be illustrated in Figure 75, 76, 77 and 78.

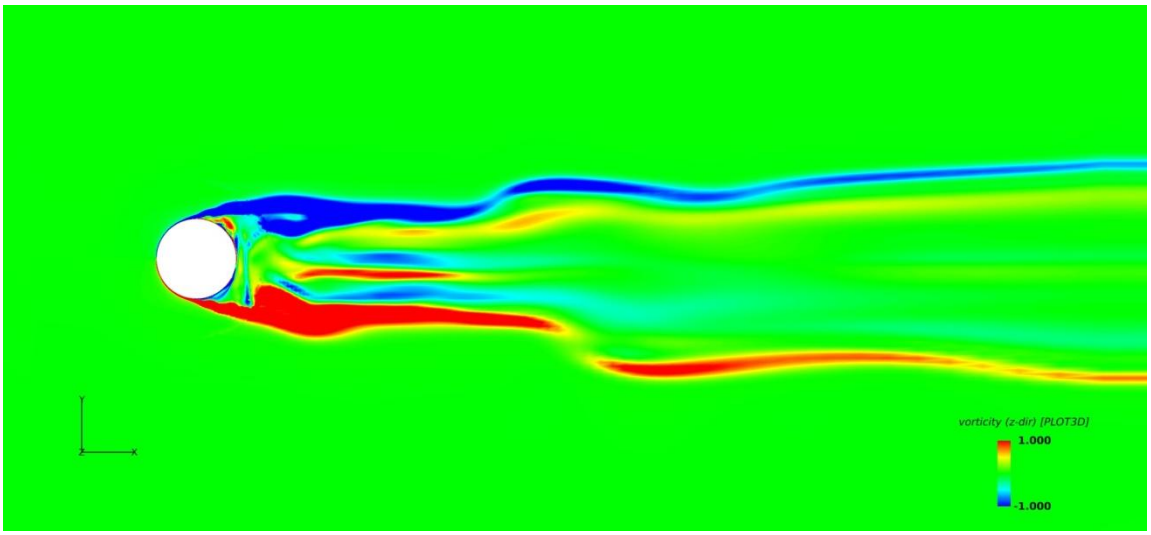

Figure 75. Vorticity Pattern with Current Velocity = 0.5m/s

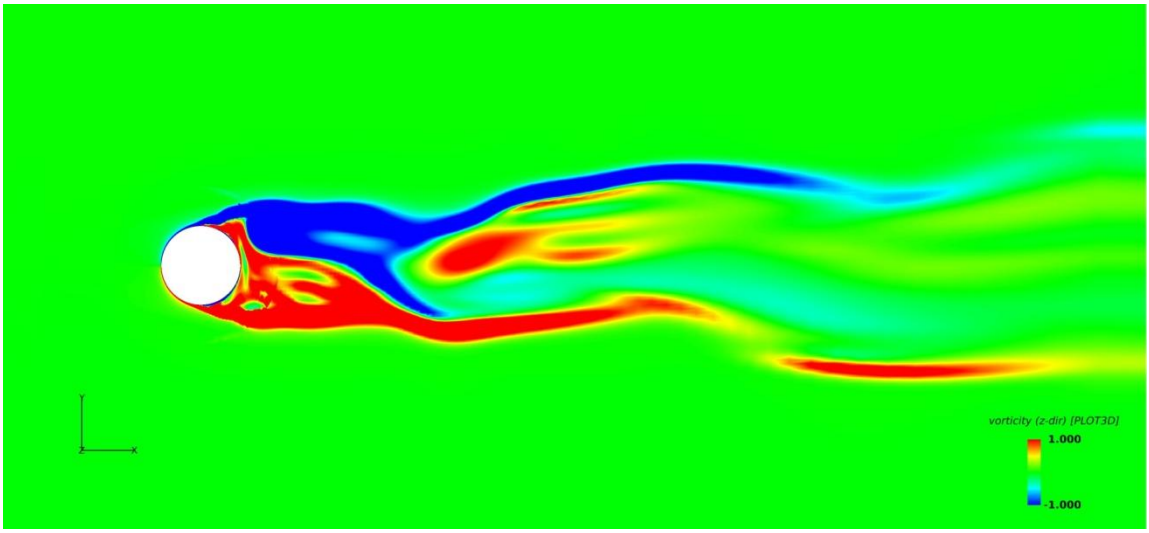

Figure 76. Vorticity Pattern with Current Velocity = 1.0m/s

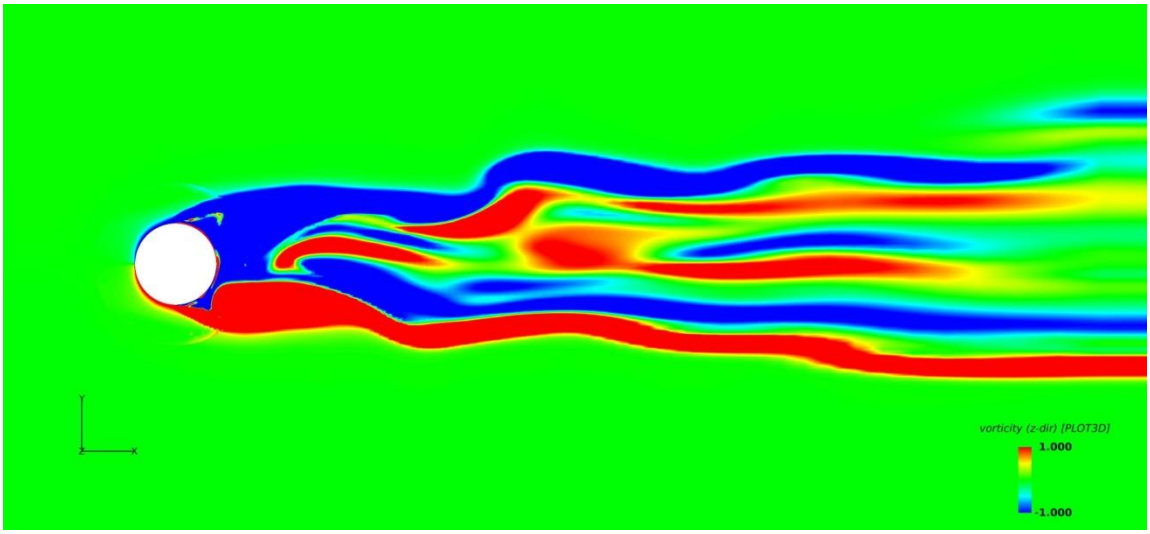

Figure 77. Vorticity Pattern with Current Velocity = 2.0m/s

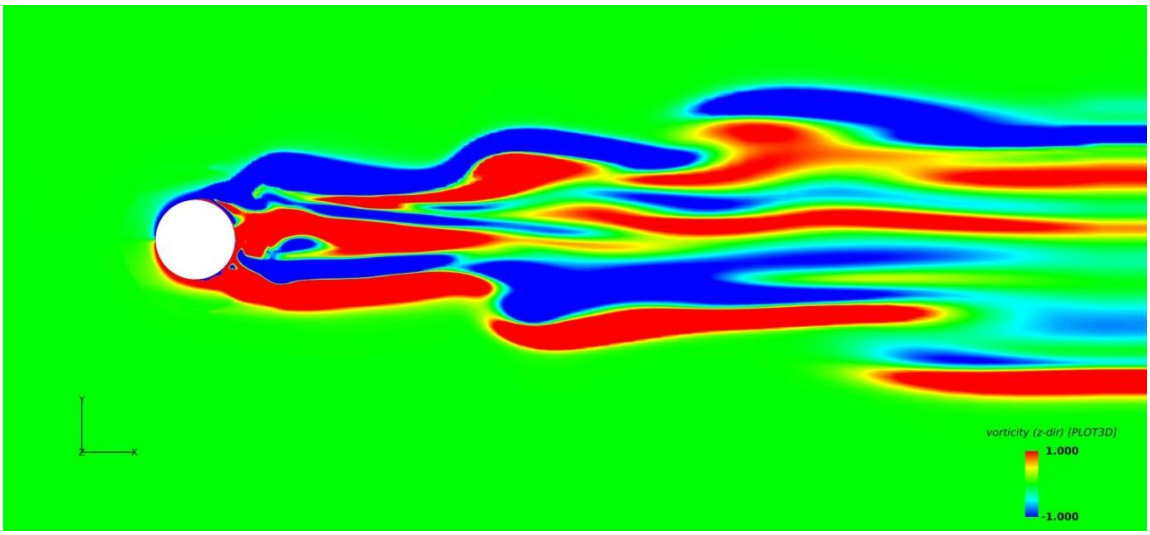

Figure 78. Vorticity Pattern with Current Velocity = 3.0m/s

Figures 75, 76, 77 and 78 illustrate the comparison of the vortex contours in z direction under four different current velocities. The location of the fluid surface is z=-1.7m. The full-scale solution time taken in the four pictures is the same, which is 1000s. From the pictures it can be seen that the areas of vortex and vortex shedding increase with the increment of the current velocity, which means that the influence of vorticity is stronger in higher current velocity than the one in lower current velocity. The composition of the vorticity pattern in z direction also becomes more complicated under the condition of higher current velocity.

The differences of the contours of vortex presented from Figure 75 to Figure 78 can directly explain the differences of displacements of the buoy in x and y directions shown in Figure 73 and Figure 74. It can be inferred that the amplitudes of oscillations in surge and sway displacements are directly related to the strength of vortices generated by uniform currents.

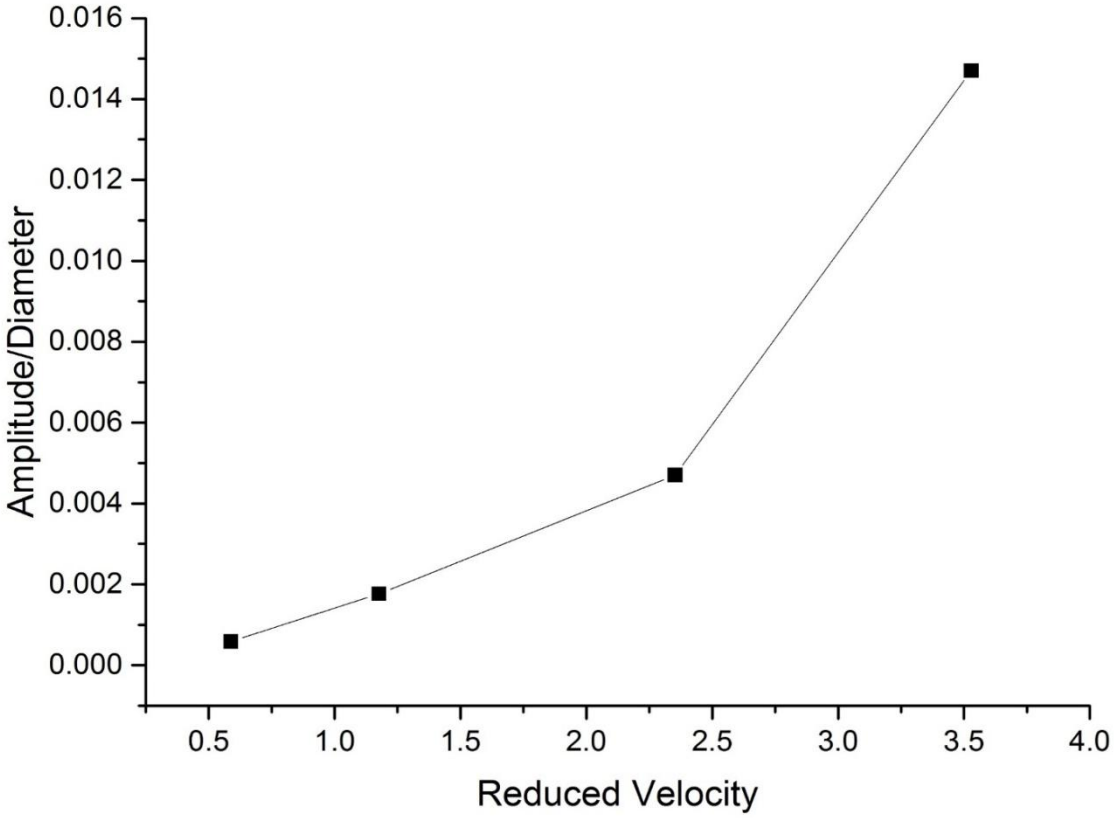

Figure 79. Amplitude/Diameter versus Reduced Velocity

Figure 79 shows the relations between the vortex-induced motion amplitude and the current velocity. From the picture it can be seen that the VIM responses of the buoy is far from the significant amplitude (0.15D) within the range of reduced velocity from 0.5 to 3.5, which means that the vibration of the buoy induced by vortex shedding is trivial compared to the buoy's diameter under the influence of current in real world.

In summary, by analyzing the dynamic responses of the CALM buoy system under the condition of different current velocities, it can be concluded that the displacement of the buoy is directly related to the current velocity. The vorticity is the

main reason for the oscillating motion in crossflow direction, while for the buoy model used in this simulation, the vortex-induced motion is so small compared to the dimension of the buoy that it has little influence on the CALM buoy system under the condition of uniform currents.

CHAPTER VI

SUMMARY AND CONCLUSION

The aim of the study is to develop a new method to simulate the hydrodynamic response of CALM buoy system. Compared to other methods used in previous study, the method in this thesis applies CFD approach (FANS code) to simulate the hydrodynamic behavior of the deep water buoy. The FANS module is coupled with a cable analysis code MOORING3D focused on the prediction of mooring lines' hydrodynamic behavior. The combination of the two modules is achieved with an interface module used for information transfer.

The procedure of the research is divided into four parts. The first step is to check the capability of FANS module and MOORING3D code separately. For the FANS module, a fixed buoy model under the condition of an uniform current is tested. For the MOORING3D part, a prescribed motion of the mooring line system is tested. The input parameters for this test comes from the output of the commercial software, Orcaflex. By comparing the results, it is verified that the FANS code and the MOORING3D code can be used for the next step. The second step is calibrating the newly established CALM buoy system in the coupled FANS/MOORING3D code. A comparison of the surge displacements in the same free-decay test simulated following three methods (coupled code, Orcaflex and model test) is made for calibration. With the model established and calibrated at the second step, an uniform current condition is introduced at the third step and the results are compared with the data obtained from the simulation by Orcaflex for

verification. With the results from the 3rd step, the coupled code method is confirmed to have the capability for accurate estimation of hydrodynamic behaviors of the CALM buoy system under the uniform current condition. The last step is to study the vortex-induced motion behavior of the CALM buoy system under the condition of different uniform currents.

To sum up, according to the results obtained from this research, it has been shown that a coupled FANS/MOORING3D method is developed to simulate the hydrodynamic behavior of the CALM buoy system accurately. Future research potential for this can consider all the 6 degrees of freedom motions, although based on the previous model tests (Cunff et al., 2007; Duggal et al., 2005), the order of heave motion displacement is relatively small compared to horizontal one under certain circumstances. The geometry of both buoy and mooring system is simplified to improve the time efficiency of calculation, which also may have some small effect on the final result. These simplifications can also be taken into account for the further research. With further development, this method is able to simulate the hydrodynamic responses of various types of offshore moored structures with different geometries accurately and efficiently.

REFERENCES

Berhault, C., Guérin, P., Le Buhan, P., Heurtier, J.M., 2004. Investigations on Hydrodynamic and Mechanical Coupling Effects for Deepwater Offloading Buoy, The Fourteenth International Offshore and Polar Engineering Conference. International Offshore and Polar Engineering Conference, Toulon, France.

Bunnik, T.H.J., Boer, G., Cozijn, J.L., Cammen, J., Haaften, E., Brake, E., 2002. Coupled Mooring Analysis and Large Scale Model Tests on a Deepwater Calm Buoy in Mild Wave Conditions, OMAE 2002: The 21st international Conference on Offshore Mechanics and Arctic Engineering, Oslo, Norway.

Chen, H.-C., Chen, C.-R., Huang, K., 2013. CFD Simulation of Vortex-induced and Wake-induced Vibrations of Dual Vertical Risers, The Twenty-third International Offshore and Polar Engineering Conference. International Society of Offshore and Polar Engineers.

Chen, H., Patel, V., 1988. Near-wall Turbulence Models for Complex Flows Including Separation. AIAA Journal 26 (6), 641-648.

Chen, H., Patel, V., 1989. The Flow around Wing-body Junctions, Symposium on Numerical and Physical Aspects of Aerodynamic Flows, 4 th, Long Beach, CA.

Chen, X., 2002. Studies on Dynamic Interaction between Deep-water Floating Structures and Their Mooring/Tendon System, Ocean Engineering. Texas A&M University, Dissertation, College Station.

Chen, X., Zhang, J., Johnson, P., Irani, M., 2000. Studies On the Dynamics of Truncated Mooring Line, The Tenth International Offshore and Polar Engineering Conference. International Offshore and Polar Engineering Conference, Seattle, USA.

Cozijn, H., Uittenbogaard, R., Brake, E., 2005. Heave, Roll and Pitch Damping of a Deepwater CALM Buoy with a Skirt, The Fifteenth International Offshore and Polar Engineering Conference. International Offshore and Polar Engineering Conference, Seoul, Korea.

Cozijn, J.L., Bunnik, T.H.J., 2004. Coupled Mooring Analysis for a Deep Water CALM Buoy, OMAE2004: 23rd International Conference on Offshore Mechanics and Arctic Engineering, Vancouver, British Columbia, Canada.

Cunff, C.L., Ryu, S., Duggal, A., Ricbourg, C., Heurtier, J.-M., Heyl, C., Liu, Y., Beauclair, O., 2007. Derivation of CALM Buoy Coupled Motion RAOs in Frequency Domain and Experimental Validation, The Seventeenth International Offshore and Polar Engineering Conference. International Society of Offshore and Polar Engineers, Lisbon, Portugal.

Duggal, A., Ryu, S., 2005. The Dynamics of Deepwater Offloading Buoys. WIT Transactions on The Built Environment 84, 10.

Garrett, D., 1982. Dynamic Analysis of Slender Rods. Journal of Energy Resources Technology 104 (4), 302-306.

Hiraishi, T., Hasegawa, I., Miyazato, I., 2008. Experimental Study on Wave-induced Motion of Offshore Observation Buoy, The Eighteenth International Offshore and Polar Engineering Conference. The International Society of Offshore and Polar Engineers, Vancouver, BC, Canada.

Huang, K., Chen, H.-C., Chen, C.-R., 2012. Vertical Riser VIV Simulation in Sheared Current. International Journal of Offshore and Polar Engineering 22 (02), 142-149.

Huang, Z.J., Santala, M.J., Wang, H., Yung, T.W., Kan, W., Sandstrom, R.E., 2005. Component Approach for Confident Predictions of Deepwater CALM Buoy Coupled Motions - Part 1: Philosophy, ASME 2005 24th International Conference on Offshore Mechanics and Arctic Engineering. International Conference on Offshore Mechanics and Arctic Engineering, Halkidiki, Greece.

Kitney, N., Brown, D.T., 2001. Experimental Investigation of Mooring Line Loading Using Large and Small-Scale Models. Journal of Offshore Mechanics and Arctic Engineering 123 (1), 1.

Lindahl, J., Sjoberg, A., 1983. Dynamic Analysis of Mooring Cables, Second International Symposium on Ocean Engineering and Ship Handling, Goteborg, Sweden.

Ma, W., Webster, W., 1994. An Analytical Approach to Cable Dynamics: Theory and User Manual. SEA GRANT PROJECT R/OE-26. Department of Naval Architecture and Offshore Engineering. University of California at Berkeley.

MARINTEK, 1989. Model Tests of A Deep Water CALM Buoy, Main Report No. 511151, Trondheim, Norway.

Meakin, R.L., 1999. Composite Overset Structured Grids. Handbook of Grid Generation, 1-20.

Pontaza, J., Chen, C., Chen, H., 2004. Chimera Reynolds-averaged Navier-Stokes Simulations of Vortex-induced Vibration of Circular Cylinders, Proc. of International ASCE Conference: Civil Engineering in the Oceans VI, pp. 166-176.

Pontaza, J., Chen, C., Chen, H., 2005. Simulation of High Reynolds Number Flow past Arrays of Circular Cylinders Undergoing Vortex-induced Vibrations, The Fifteenth International Offshore and Polar Engineering Conference. International Society of Offshore and Polar Engineers.

Ricbourg, C., Berhault, C., Camhi, A., Lécuyer, B., Marcer, R., R.D., P., 2006. Numerical and Experimental Investigations on Deepwater CALM Buoys Hydrodynamics Loads, Offshore Technology Conference.

Ryu, S., Duggal, A.S., Heyl, C.N., Liu, Y., 2005. Coupled Analysis of Deepwater Oil Offloading Buoy And Experimental Verification, The Fifteenth (2005) International Offshore and Polar Engineering Conference, Seoul, Korea.

Ryu, S., Duggal, A.S., Heyl, C.N., Liu, Y., 2006. Prediction of Deepwater Oil Offloading Buoy Response and Experimental Validation. International Journal of Offshore and Polar Engineering 16 (3), 1-7.

Sagrilo, L.V.S., Siqueira, M.Q., Ellwanger, G.B., Lima, E.C.P., Ferreira, M.D.A.S., Mourelle, M.M., 2002. A Coupled Approach for Dynamic Analysis of CALM Systems. Applied Ocean Research 24, 47–58.

Salem, A.G., Ryu, S., Duggal, A.S., Datla, R.V., 2012. Linearization of Quadratic Drag to Estimate CALM Buoy Pitch Motion in Frequency-Domain and Experimental Validation. Journal of Offshore Mechanics and Arctic Engineering 134 (1), 011305.

Williams, A.N., McDougal, W.G., 2013. Experimental Validation of a New Shallow Water CALM Buoy Design, ASME 2013 32nd International Conference on Ocean, Offshore and Arctic Engineering, Nantes, France.

Woodburn, P., Gallagher, P., Naciri, M., Borleteau, J.-P., 2005. Coupled CFD Simulation of the Response of a CALM Buoy in Waves, OMAE2005: 24th International Conference on Offshore Mechanics and Arctic Engineering, Halkidiki, Greece.

Zhao, L., 2014. Private Communication.